An Adaptive Control System for an Accelerating Rotor Supported by Active Magnetic Bearings under Unbalance Disturbances

by

Xianglin Wang

A thesis submitted to the Graduate Faculty of
Auburn University
in partial fulfillment of the
requirements for the Degree of
Master of Science

Auburn, Alabama
August 6, 2016

Keywords: active magnetic bearing, transient rotor, vibration control,
adaptive disturbance rejection

Copyright 2016 by Xianglin Wang

Approved by

George T. Flowers, Chair, Professor of Mechanical Engineering
David M. Bevly, Professor of Mechanical Enginnering
John Y. Hung, Professor of Electrical and Computer Engineering

Abstract

This thesis describes an adaptive control system capable of rejecting unbalance disturbances for an accelerating rotor supported by active magnetic bearings (AMBs). The control of accelerating rotor during start-up and shut-down for rotating machines with AMBs is difficult, especially when the rotor has strong unbalance, which results in sinusoidal disturbances of time-varying frequency and time-varying amplitude. A stabilizing controller alone is not able to obtain a satisfying dynamic performance in this situation. Therefore, unbalance disturbance rejection control is needed. The research work on this topic is mostly based on steady-state rotor model, therefore, those methods are not applicable during rotor acceleration.

In this thesis, a transient rigid rotor model is first developed and then used for controller design and stability analysis. The adaptive control system, which falls into the category of model reference adaptive system (MRAS), includes a PD-typed controller for stabilizing the system, and an adaptive disturbance rejection (ADR) controller for rejecting disturbances. The ADR controller utilizes rotor speed measurement, which is a piece of known information for most rotating machines, to construct a feedforward regressor vector, and makes the rejection of unbalance disturbances during rotor acceleration possible. It is proved by Lyapunov theory that the adaptive control system is asymptotically stable. Dynamic performances of the adaptive control system are shown by computer simulation.

Acknowledgments

I would like to acknowledge my advisor, George T. Flowers for his advice in completing this work. I would like to thank John Hung, David Bevly, Subhash Sinha and Andrew Sinclair for providing me with great courses on Dynamics and Control in Auburn University. I would thank my parents, Yongqun He and Ji Wang, for trusting their son and letting him explore America. I also would like to thank my girlfriend Yalan Bi for her support.

Contents

List of Figures

List of Tables

Chapter 1

Introduction and literature review

Active magnetic bearing (AMB) system, which use electromagnetic forces to support rotating parts in machines, are adopted into more and more industrial applications. In Chapter 1 of [4], a survey is conducted to show these exciting applications.

Because the nature of open loop instability, it is necessary for an AMB system to have feedback control. In [1], decentralized PD controller, LQR controller and cross feedback controller are compared. It is found that when using LQR control, gain scheduling is necessary to maintain the stability of closed loop system. And cross feedback controller, with its ability to attenuate gyroscopic effects actively, leads to a better system performance. However, the discussion is based on steady-state rotor, therefore, how to choose control design parameters considering the accelerating process is not mentioned.

Moreover, because unbalance exists in every rotor in real world, unbalance disturbance rejection control is needed to obtain a better system performances, especially when unbalance is strong and rotor speed is high. In [10], an adaptive disturbance rejection (ADR) controller is successfully implemented by A. Matras on an AMB test rig. In [3], K. Barber uses the adaptive gains of the ADR controller to monitor the health of rotor supported by AMBs. Once again, both of these works are based on steady-state rotor. However, if the disturbance rejection control can only work for steady-state rotor, then there will be no way to shut down or start up the machine. Therefore, the control of AMB systems during acceleration must be investigated.

During acceleration, the control problem gets much more complicated. Firstly, the rotor becomes transient, so the system is time-varying instead of time invariant. In addition, the unbalance disturbance is of fast-varying frequency and magnitude. In [14], Zhou et al. try to

include the dynamics of imbalance mass into a transient rotor model, and use this augmented system model to estimate the imbalance mass, and then reject the unbalance disturbances. But it is find that this augmented model is of very weak observability and even unobservable under certain choice of model data.

In [6], Fuentes and Balas design an adaptive controller which is able to reject sinusoidal disturbances of fixed frequency and fixed magnitude. The key of this controller is to include the sinusoidal functions with the frequencies of possible disturbance sources into a regressor vector. Then the adaptation mechanism can calculate control forces with feedback and the regressor vector to reject the disturbances. This method is very suitable for controlling structural vibration, where the excitation is a combination of several sinusoidal functions of fixed frequency and fixed amplitude. However, for rotating machines, the unbalance disturbances during acceleration is of time-varying frequency and time-varying amplitude. A finite number of sinusoidal functions in regressor vector can not correctly represent the disturbances. An attempt to use multiple sinusoidal functions in the regressor vector of adaptive controller can be found in [8].

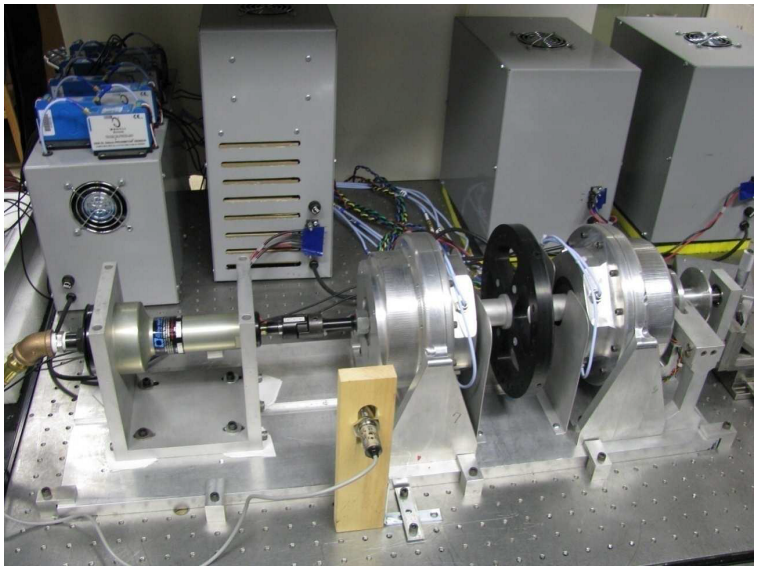

Figure 1.1: An AMB test rig in Rotating Machines Laboratory (RML), Auburn University [9]

In this thesis, a theoretical study on the control of a transient AMB system based on model data of the test rig in Auburn University (shown in Fig. 1.1) will be conducted. In Chapter 2, equations of motion will be developed using Lagrange equation. Without further introducing control, a desired closed loop transient AMB system is provided. In Chapter 3, rotordynamics analysis will be performed analytically and computationally for the desired system. Then desired system parameters will be selected based on the analysis. Using local PD controller and centralized PD controller to realize the desired closed loop system will be discussed. In Chapter 4, an adaptive controller for the rejection of sinusoidal disturbances with time-varying frequency and time-varying amplitude will be designed using Lyapunov theory. The idea of using sinusoidal functions in regressor vector in [6] will be extended. Instead of using sinusoidal functions of fixed frequency and magnitude, the sinusoidal functions of time-varying amplitude and frequency will be constructed by rotor speed measurement. With taking the full advantage of rotor speed measurement, the unbalance disturbances can be rejected in AMB systems during fast acceleration.

Chapter 2

Dynamic modeling for a transient AMB system

2.1 Equations of motion for a transient rotor without support

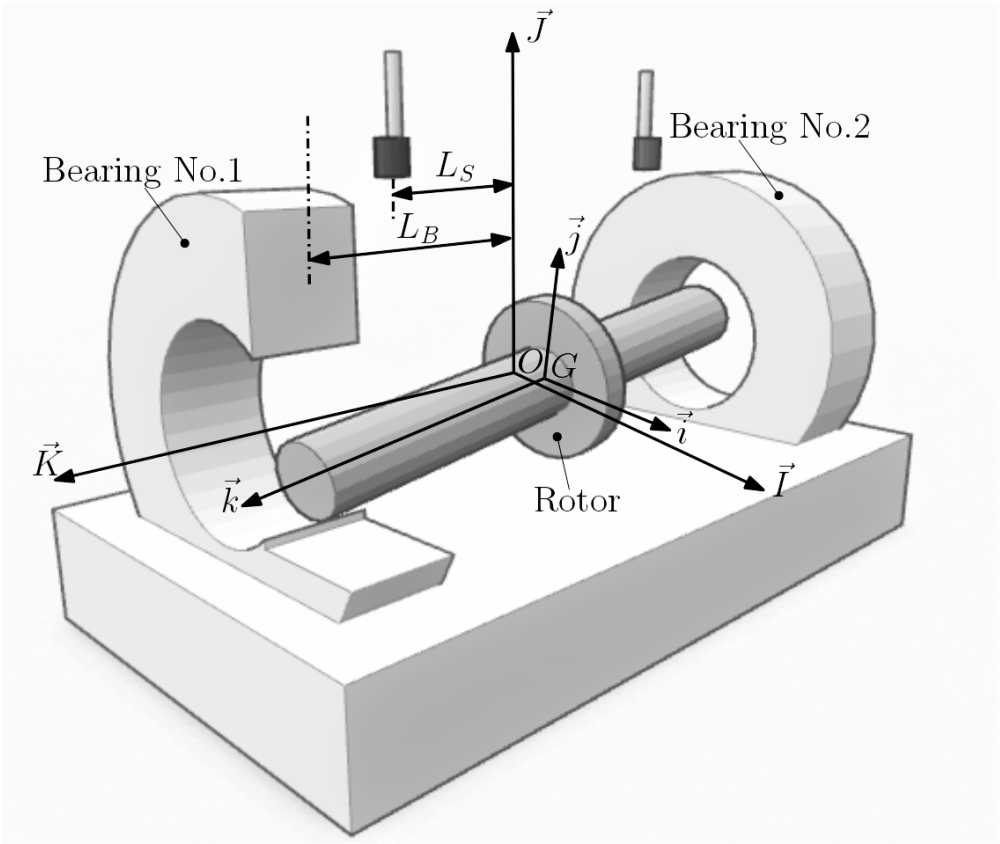

Figure 2.1: Diagram for an AMB system

A 4 degree-of-freedom rigid Jeffcott rotor [13] is shown in Fig.2.1. Let O be the origin of a space-fixed coordinate system $O-XYZ$. Let G be the center of mass of the rotor and the origin of a rotor-fixed coordinate system $G-xyz$. Displacement of the rotor consists of rotational displacement and translational displacement. The rotational displacement can be described by the following sequences

1. Initially, $O - XYZ$ coincides with $G - xyz$.

2. The rotor rotates α rad about Y axis. Let the location of $G-xyz$ be the initial location of an intermediate coordinate system $O - x'y'z'$.

3. The rotor rotates β rad about x' axis.

4. The rotor rotates ψ rad about z axis.

The translational displacement can be described by $\vec{r}_G = \vec{r}_{G/O} = (X,\ Y)$. Note that the translational displacement along Z axis is neglected.
The angular velocity of the rotor is given by

$$\begin{aligned}\vec{\Omega} &= \dot{\alpha}\vec{J} + \dot{\beta}\vec{i'} + \dot{\psi}\vec{k} \\ &= \dot{\beta}\vec{i} + \dot{\alpha}\cos\beta\vec{j} + (\dot{\psi} - \dot{\alpha}\sin\beta)\vec{k}\end{aligned} \tag{2.1}$$

The translational velocity of the rotor is given by

$$\vec{v}_G = \dot{X}\vec{I} + \dot{Y}\vec{J} \tag{2.2}$$

Let the angular momentum of the rotor about G be $\vec{H}_G$, the kinetic energy of this 'free' rotor (rotor with no support) is given by

$$T = \frac{1}{2}m\vec{v}_G \cdot \vec{v}_G + \frac{1}{2}\vec{\Omega} \cdot \vec{H}_G \tag{2.3}$$

which can be calculated using matrix form

$$\begin{aligned} T =& \frac{1}{2}m \begin{bmatrix} \dot{X} & \dot{Y} \end{bmatrix} \begin{bmatrix} \dot{X} \\ \dot{Y} \end{bmatrix} + \frac{1}{2} \begin{bmatrix} \dot{\beta} & \dot{\alpha}\cos\beta & (\dot{\psi} - \dot{\alpha}\sin\beta) \end{bmatrix} \begin{bmatrix} I_T & 0 & 0 \\ 0 & I_T & 0 \\ 0 & 0 & I_P \end{bmatrix} \begin{bmatrix} \dot{\beta} \\ \dot{\alpha}\cos\beta \\ (\dot{\psi} - \dot{\alpha}\sin\beta) \end{bmatrix} \\ =& \frac{1}{2}m\dot{X}^2 + \frac{1}{2}m\dot{Y}^2 + \frac{1}{2}I_T\dot{\beta}^2 + \frac{1}{2}I_T(\cos\beta)^2\dot{\alpha}^2 + \frac{1}{2}I_P\dot{\psi}^2 + \frac{1}{2}I_P\dot{\alpha}^2(\sin\beta)^2 - I_P\dot{\psi}\dot{\alpha}\sin\beta \end{aligned} \tag{2.4}$$

Assuming α and β are small and discarding third order and higher order terms, yields

$$T = \frac{1}{2}m\dot{X}^2 + \frac{1}{2}m\dot{Y}^2 + \frac{1}{2}I_T\dot{\beta}^2 + \frac{1}{2}I_T\dot{\alpha}^2 + \frac{1}{2}I_P\dot{\psi}^2 - I_P\dot{\psi}\dot{\alpha}\beta \tag{2.5}$$

Treating ψ as a system parameter instead of a dynamic variable, the rotor has four degrees of freedom, which can be described by the generalized coordinates

$$q = \begin{bmatrix} \alpha \\ X \\ \beta \\ Y \end{bmatrix} \tag{2.6}$$

Using *Lagrange equation* [7]

$$\frac{\partial T}{\partial q_i} + \frac{d}{dt}\frac{\partial T}{\partial \dot{q}_i} = Q_i \tag{2.7}$$

for each generalized coordinate.

Equations of motion in matrix form is given by

$$\underbrace{\begin{bmatrix} I_T & 0 & 0 & 0 \\ 0 & m & 0 & 0 \\ 0 & 0 & I_T & 0 \\ 0 & 0 & 0 & m \end{bmatrix}}_{M} \begin{bmatrix} \ddot{\alpha} \\ \ddot{X} \\ \ddot{\beta} \\ \ddot{Y} \end{bmatrix} + \underbrace{\begin{bmatrix} 0 & 0 & -I_P\dot{\psi} & 0 \\ 0 & 0 & 0 & 0 \\ I_P\dot{\psi} & 0 & 0 & 0 \\ 0 & 0 & 0 & 0 \end{bmatrix}}_{G(\dot{\psi})} \begin{bmatrix} \dot{\alpha} \\ \dot{X} \\ \dot{\beta} \\ \dot{Y} \end{bmatrix} = \underbrace{\begin{bmatrix} Q_1 \\ Q_2 \\ Q_3 \\ Q_4 \end{bmatrix}}_{Q} \tag{2.8}$$

where Q_i is the generalized force corresponding to each generalized coordinate; M is the mass matrix; G is the gyroscopic matrix.

2.2 Unbalance excitation forces

One way to model unbalance in a rotor is to treat it as an imbalance mass in an arbitrary location (u_z, d, ψ_0) of the rotor, as shown in Fig.2.2

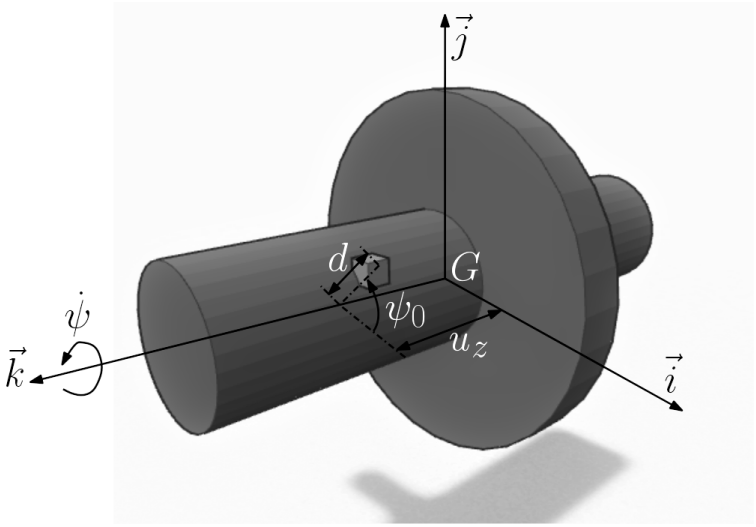

Figure 2.2: Diagram for a rotor attached with imbalance mass

2.2.1 Kinematic analysis

In a rotor-fixed coordinate system, the displacement of imbalance mass can be described by

$$r = d\cos(\psi + \psi_0)i + d\sin(\psi + \psi_0)j + u_z k \tag{2.9}$$

During spinning, the magnitude of r doesn't change. Only the direction of r changes. The velocity of imbalance mass can be written as

$$v = \frac{dr}{dt} = \dot{\psi} \times r \tag{2.10}$$

Taking derivative of velocity with respect to time, the acceleration of imbalance mass is given by

$$\begin{aligned} a &= \frac{dv}{dt} \\ &= \dot{\psi} \times (\dot{\psi} \times \dot{r}) + \ddot{\psi} \times r \\ &= \dot{\psi}k \times [\dot{\psi}k \times (d\cos(\psi + \psi_0)i + d\sin(\psi + \psi_0)j)] + \ddot{\psi}k \times [d\cos(\psi + \psi_0)i + d\sin(\psi + \psi_0)j] \\ &= -[d\dot{\psi}^2 \cos(\psi + \psi_0) + d\ddot{\psi}\sin(\psi + \psi_0)]i + [d\ddot{\psi}\cos(\psi + \psi_0) - d\dot{\psi}^2 \sin(\psi + \psi_0)]j \end{aligned} \tag{2.11}$$

2.2.2 Kinetic analysis

By *Newton's third law*, to sustain the motion of imbalance mass, the unbalance force acting on rotor is

$$f_u = -m_u a \tag{2.12}$$

where m_u is the mass of imbalance mass, a is the acceleration from Eq. 2.11.
Defining $u_x = d\cos\phi_0$ and $u_y = d\sin\phi_0$, Eq. 2.12 becomes

$$\begin{aligned} f_u = &(m_u u_x \dot{\psi}^2 \cos\psi - m_u u_y \dot{\psi}^2 \sin\psi + m_u u_x \ddot{\psi}\sin\psi + m_u u_y \ddot{\psi}\cos\psi)i \\ &+ (m_u u_x \dot{\psi}^2 \sin\psi + m_u u_y \dot{\psi}^2 \cos\psi - m_u u_x \ddot{\psi}\cos\psi + m_u u_y \ddot{\psi}\sin\psi)j \end{aligned} \tag{2.13}$$

The displacement of imbalance mass can be written as

$$r_u = u_x i + u_y j + u_z k \tag{2.14}$$

Then the moment of unbalance force can be written as

$$
\begin{aligned}
M_u =& r_u \times f_u \\
=& (u_x i + u_y j + u_z k) \\
& \times [(m_u u_x \dot{\psi}^2 \cos\psi - m_u u_y \dot{\psi}^2 \sin\psi + m_u u_x \ddot{\psi} \sin\psi + m_u u_y \ddot{\psi} \cos\psi) i \\
& + (m_u u_x \dot{\psi}^2 \sin\psi + m_u u_y \dot{\psi}^2 \cos\psi - m_u u_x \ddot{\psi} \cos\psi + m_u u_y \ddot{\psi} \sin\psi) j] \\
=& + (m_u u_x^2 \dot{\psi}^2 \sin\psi + m_u u_y u_x \dot{\psi}^2 \cos\psi) k \\
& - (m_u u_x u_y \dot{\psi}^2 \cos\psi - m_u u_y^2 \dot{\psi}^2 \sin\psi) k \\
& + (-m_u u_x^2 \ddot{\psi} \cos\psi + m_u u_y u_x \ddot{\psi} \sin\psi) k \\
& - (m_u u_x u_y \ddot{\psi} \sin\psi + m_u u_y^2 \ddot{\psi} \cos\psi) k \\
& + (m_u u_x u_z \dot{\psi}^2 \cos\psi - m_u u_y u_z \dot{\psi}^2 \sin\psi) j \\
& + (m_u u_x u_z \ddot{\psi} \sin\psi + m_u u_y u_z \ddot{\psi} \cos\psi) j \\
& - (m_u u_x u_z \dot{\psi}^2 \sin\psi + m_u u_y u_z \dot{\psi}^2 \cos\psi) i \\
& + (m_u u_x u_z \ddot{\psi} \cos\psi - m_u u_y u_z \ddot{\psi} \sin\psi) i
\end{aligned}
\tag{2.15}
$$

2.2.3 Associating unbalance excitation forces with generalized coordinates

For the generalized coordinates $q = (\alpha\ X\ \beta\ Y)^\top$, the associated unbalance excitation forces can be written as

$$\begin{aligned} Q_u &= \begin{bmatrix} m_u u_x u_z & m_u u_y u_z \\ m_u u_x & m_u u_y \\ -m_u u_y u_z & m_u u_x u_z \\ m_u u_y & -m_u u_x \end{bmatrix} \left(\underbrace{\begin{bmatrix} \dot{\psi}^2 \cos\psi \\ -\dot{\psi}^2 \sin\psi \end{bmatrix}}_{\text{speed-related term}} + \underbrace{\begin{bmatrix} \ddot{\psi} \sin\psi \\ -\ddot{\psi} \cos\psi \end{bmatrix}}_{\text{acceleration-related term}} \right) \\ &= \underbrace{\begin{bmatrix} m_u u_x u_z & m_u u_y u_z \\ m_u u_x & m_u u_y \\ -m_u u_y u_z & m_u u_x u_z \\ m_u u_y & -m_u u_x \end{bmatrix}}_{B_d} \underbrace{\begin{bmatrix} \dot{\psi}^2 \cos\psi + \ddot{\psi} \sin\psi \\ -\dot{\psi}^2 \sin\psi + \ddot{\psi} \cos\psi \end{bmatrix}}_{u_d} \end{aligned} \tag{2.16}$$

where u_d is the disturbance vector, which consists of speed-induced term and acceleration-induced term; B_d is the disturbance input path matrix.

Unbalance ratio

Unbalance ratio is defined as following to parameterize the strength of unbalance

$$c_u = \frac{m_u}{m} \tag{2.17}$$

2.3 Electromagnetic forces

2.3.1 Linearization of electromagnetic forces

The function of a electromagnetic actuator in AMB systems is to generate electromagnetic forces to control the motion of rotor. Fig.2.3 shows the diagram for one axis of a bearing coordinates, which has one pair of electromagnets. Note that the angle between direction of gravity force and this axis of bearing coordinates is 45 degrees for this particular setup of electromagnets.

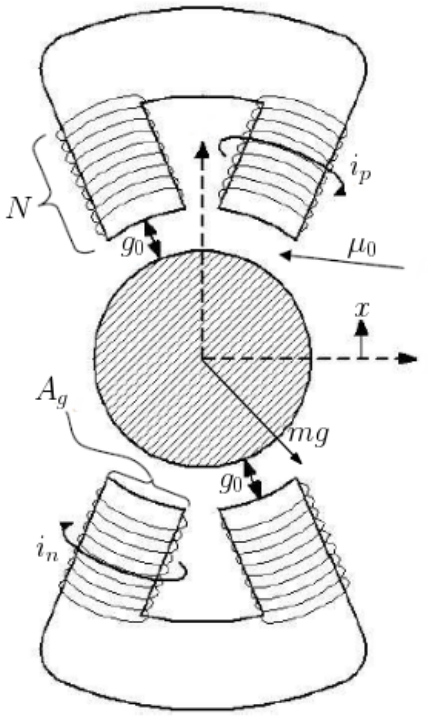

Figure 2.3: Diagram for one axis of bearing coordinates

Define

$$Z = \frac{\mu_0 A N^2}{4} \tag{2.18}$$

where μ_0 is the permeability of free space, A is the electromagnet pole face area and N is the number of coil turns.

The electromagnetic force along this axis is given by

$$F = Z\frac{i_p^2}{x_p^2} - Z\frac{i_n^2}{x_n^2} \tag{2.19}$$

Bias current is used. i_{bp} is the bias current for the electromagnet on the top, or along the *positive* direction of the axis. i_{bn} is the bias current for electromagnet on the bottom, or along the *negative* direction of the axis. Then Eq. 2.19 can be written as

$$F = Z\frac{(i_{bp} + i_c)^2}{(g_o - x)^2} - Z\frac{(i_{bn} - i_c)^2}{(g_o + x)^2} \tag{2.20}$$

Linearizing $F(i_p, i_n, x_p, x_n)$ about operating point $(i_{pb}, i_{nb}, g_o, g_o)$ by *Taylor series*, yields

$$\begin{aligned} F(i_p, i_n, x_p, x_n) &= F(i_{pb}, i_{nb}, g_o, g_o) + \frac{\partial F}{\partial i_p}i_c + \frac{\partial F}{\partial i_n}i_c + \frac{\partial F}{\partial x_p}(-x) + \frac{\partial F}{\partial x_n}(x) \\ &= \frac{2Zi_{bp}}{g_o^2}i_c + \frac{2Zi_{bn}}{g_o^2}i_c + \frac{2Z(i_{bp}^2 + i_{bn}^2)}{g_o^3}x \\ &= \frac{2Z(i_{bp} + i_{bn})}{g_o^2}i_c + \frac{2Z(i_{bp}^2 + i_{bn}^2)}{g_o^3}x \end{aligned} \tag{2.21}$$

Defining *force/current factor* $k_i = \frac{2Z(i_{bp}+i_{bn})}{g_o^2}$ and *force/displacement factor* $k_s = -\frac{2Z(i_{bp}^2+i_{bn}^2)}{g_o^3}$, Eq. 2.21 becomes

$$F(i_p, i_n, x_p, x_n) = F(i_{pb}, i_{nb}, g_o, g_o) + k_i i_c - k_s x \tag{2.22}$$

Ideally, $F(i_{pb}, i_{nb}, g_o, g_o)$ will be canceled by the gravity force acting on the rotor, then the scalar linearized electromagnetic force in one axis along bearing coordinates can be described by

$$f_m = k_i i_c - k_s x \tag{2.23}$$

2.3.2 Calculation of bias current

By static analysis, to provide the static force to levitate the rotor in non-spinning situation, one pair of electromagnets need to provide

$$F_{need} = \frac{mg}{2}\frac{\sqrt{2}}{2} \tag{2.24}$$

Then the bias current i_{bp} and i_{bn} need to satisfy

$$\begin{aligned} F_{static} &= Z\frac{i_{bp}^2}{g_0^2} - Z\frac{i_{bn}^2}{g_0^2} \\ &= F_{need} \end{aligned} \tag{2.25}$$

Therefore, once i_{bp} is chosen, i_{bn} can be calculated by

$$i_{bn} = \sqrt{i_{bp}^2 - \frac{g_0^2 F_{need}}{Z}} \tag{2.26}$$

And then k_s and k_i can be calculated from i_{bp} and i_{bn}.

2.3.3 Associating electromagnetic forces with generalized coordinates

For the generalized coordinates $q = (\alpha\ X\ \beta\ Y)^\top$, the associated electromagnetic forces can be written as

$$
\begin{aligned}
Q_m = \underbrace{\begin{bmatrix} L_B & -L_B & 0 & 0 \\ 1 & 1 & 0 & 0 \\ 0 & 0 & -L_B & L_B \\ 0 & 0 & 1 & 1 \end{bmatrix}}_{B} \Bigg(& - \underbrace{\begin{bmatrix} k_s & 0 & 0 & 0 \\ 0 & k_s & 0 & 0 \\ 0 & 0 & k_s & 0 \\ 0 & 0 & 0 & k_s \end{bmatrix}}_{K_s} \underbrace{\begin{bmatrix} L_B & -L_B & 0 & 0 \\ 1 & 1 & 0 & 0 \\ 0 & 0 & -L_B & L_B \\ 0 & 0 & 1 & 1 \end{bmatrix}^\top}_{B^\top} \begin{bmatrix} \alpha \\ X \\ \beta \\ Y \end{bmatrix} \\
& + \underbrace{\begin{bmatrix} k_i & 0 & 0 & 0 \\ 0 & k_i & 0 & 0 \\ 0 & 0 & k_i & 0 \\ 0 & 0 & 0 & k_i \end{bmatrix}}_{K_i} \begin{bmatrix} i_{c1x} \\ i_{c2x} \\ i_{c1y} \\ i_{c2y} \end{bmatrix} \Bigg) \\
& = B(-K_s B^\top q + K_i i_c)
\end{aligned}
\tag{2.27}
$$

where B is the input path matrix; K_s is the force/displacement factor matrix; K_i is the force/current factor matrix; i_c is the control current vector.

Control-to-bias ratio

Control current i_c can not be larger than bias current i_b, or the total current becomes a negative value. Also, i_c need to be small compared to i_b to avoid current saturation as well as to maintain the validation of the linearized electromagnetic force model. Therefore, a control-to-bias ratio for a chosen time period is defined as

$$\text{control-to-bias ratio} = \frac{\max(i_c)}{i_b} \tag{2.28}$$

to detect the consumption of control current. In the computer simulation and experiment of this thesis, control-to-bias ratio will be calculated in every 0.5 seconds.

Neglecting the dynamics of power amplifier

In the following discussion, the dynamics of electromagnetic actuator will be neglected to simplify the control problem. Therefore, control current is assumed to be directly provided by the controller, without any phase and amplitude changes through the actuator.

2.4 An open loop transient AMB system

Associating the electromagnetic forces and unbalance excitation forces with each generalized coordinate, the equations of motion for an open loop transient AMB system is given by

$$M\ddot{q} + G(\dot{\psi})\dot{q} = B(-K_s B^\top q + K_i i_c) + B_d u_d$$

$$M\ddot{q} + G(\dot{\psi})\dot{q} + BK_s B^\top q = BK_i i + B_d u_d$$

$$\begin{aligned}
&\begin{bmatrix} \ddot{\alpha} \\ \ddot{X} \\ \ddot{\beta} \\ \ddot{Y} \end{bmatrix} + \begin{bmatrix} 0 & 0 & -\frac{I_P\dot{\psi}}{I_T} & 0 \\ 0 & 0 & 0 & 0 \\ \frac{I_P\dot{\psi}}{I_T} & 0 & 0 & 0 \\ 0 & 0 & 0 & 0 \end{bmatrix} \begin{bmatrix} \dot{\alpha} \\ \dot{X} \\ \dot{\beta} \\ \dot{Y} \end{bmatrix} + \begin{bmatrix} \frac{2k_s L_B^2}{I_T} & 0 & 0 & 0 \\ 0 & \frac{2k_s}{m} & 0 & 0 \\ 0 & 0 & \frac{2k_s L_B^2}{I_T} & 0 \\ 0 & 0 & 0 & \frac{2k_s}{m} \end{bmatrix} \begin{bmatrix} \alpha \\ X \\ \beta \\ Y \end{bmatrix} \\
&= \begin{bmatrix} \frac{L_B k_i}{I_T} & -\frac{L_B k_i}{I_T} & 0 & 0 \\ \frac{k_i}{m} & \frac{k_i}{m} & 0 & 0 \\ 0 & 0 & -\frac{L_B k_i}{I_T} & \frac{L_B k_i}{I_T} \\ 0 & 0 & \frac{k_i}{m} & \frac{k_i}{m} \end{bmatrix} \begin{bmatrix} i_{c1x} \\ i_{c2x} \\ i_{c1y} \\ i_{c2y} \end{bmatrix} + \begin{bmatrix} \frac{m_u u_x u_z}{I_T} & \frac{m_u u_y u_z}{I_T} \\ \frac{m_u u_x}{m} & \frac{m_u u_y}{m} \\ -\frac{m_u u_y u_z}{I_T} & \frac{m_u u_x u_z}{I_T} \\ \frac{m_u u_y}{m} & -\frac{m_u u_x}{m} \end{bmatrix} \begin{bmatrix} \dot{\psi}^2 \cos\psi + \ddot{\psi}\sin\psi \\ -\dot{\psi}^2 \sin\psi + \ddot{\psi}\cos\psi \end{bmatrix}
\end{aligned} \tag{2.29}$$

In state variable description, it can be written as

$$\begin{aligned}
\dot{x} &= \underbrace{\begin{bmatrix} \varnothing & I \\ -M^{-1}BK_sB^\top & -M^{-1}G(\dot{\psi}) \end{bmatrix}}_{A_{ss}(\dot{\psi})} x + \underbrace{\begin{bmatrix} \varnothing \\ M^{-1}BK_i \end{bmatrix}}_{B_{ss}} i + \underbrace{\begin{bmatrix} \varnothing \\ M^{-1}B_d \end{bmatrix}}_{B_{d,ss}} u_d \\
y &= \underbrace{\begin{bmatrix} C & \varnothing \end{bmatrix}}_{C_{ss}} x
\end{aligned} \tag{2.30}$$

where

$$\dot{\psi} = \begin{cases} a(t - t_0), & t_0 < t < t_0 + t_a \\ at_a, & t_0 + t_a \leq t < \infty \end{cases}$$

Chapter 3

Stabilizing control design

As one of the two components for the adaptive control system, a baseline stabilizing controller need to be designed prior to the adaptive disturbance rejection controller. In this chapter, the design procedures of stabilizing controller for transient AMB system are presented. In the first part, a desired form of closed loop system is introduced. Dynamic performance of the closed loop system is discussed with respect to the choice of system parameters. Stability of the closed loop system is proved using Lyapunov theory. In the second part, two PD-typed stabilizing controllers are presented for realizing the desired closed loop system.

3.1 A desired closed loop transient AMB system

Without further introducing feedback control, a desired closed loop transient AMB system is assumed to have the form of

$$\begin{bmatrix} \ddot{\alpha} \\ \ddot{X} \\ \ddot{\beta} \\ \ddot{Y} \end{bmatrix} + \underbrace{\begin{bmatrix} 2\zeta^{con}\omega_n^{con} & 0 & -P\dot{\psi} & 0 \\ 0 & 2\zeta^{cyl}\omega_n^{cyl} & 0 & 0 \\ P\dot{\psi} & 0 & 2\zeta^{con}\omega_n^{con} & 0 \\ 0 & 0 & 0 & 2\zeta^{cyl}\omega_n^{cyl} \end{bmatrix}}_{M^{-1}(D+G(\dot{\psi}))} \begin{bmatrix} \dot{\alpha} \\ \dot{X} \\ \dot{\beta} \\ \dot{Y} \end{bmatrix} + \underbrace{\begin{bmatrix} (\omega_n^{con})^2 & 0 & 0 & 0 \\ 0 & (\omega_n^{cyl})^2 & 0 & 0 \\ 0 & 0 & (\omega_n^{con})^2 & 0 \\ 0 & 0 & 0 & (\omega_n^{cyl})^2 \end{bmatrix}}_{M^{-1}K} \begin{bmatrix} \alpha \\ X \\ \beta \\ Y \end{bmatrix}$$
$$= \begin{bmatrix} \frac{m_u u_x u_z}{I_T} & \frac{m_u u_y u_z}{I_T} \\ \frac{m_u u_x}{m} & \frac{m_u u_y}{m} \\ -\frac{m_u u_y u_z}{I_T} & \frac{m_u u_x u_z}{I_T} \\ \frac{m_u u_y}{m} & -\frac{m_u u_x}{m} \end{bmatrix} \begin{bmatrix} \dot{\psi}^2\cos\psi + \ddot{\psi}\sin\psi \\ -\dot{\psi}^2\sin\psi + \ddot{\psi}\cos\psi \end{bmatrix} \tag{3.1}$$

where

$$\dot{\psi} = \begin{cases} a(t-t_0), & t_0 < t < t_0 + t_a \\ at_a, & t_0 + t_a \le t < \infty \end{cases}$$

In state variable description, it can be written as

$$\begin{aligned}\dot{x} &= \underbrace{\begin{bmatrix} \varnothing & I \\ -M^{-1}K & -M^{-1}(G(\dot{\psi})+D) \end{bmatrix}}_{A_{cl,ss}(\dot{\psi})} x + \underbrace{\begin{bmatrix} \varnothing \\ M^{-1}BK_i \end{bmatrix}}_{B_{ss}} i + \underbrace{\begin{bmatrix} \varnothing \\ M^{-1}B_d \end{bmatrix}}_{B_{d,ss}} u_d \\ y &= \underbrace{\begin{bmatrix} C & \varnothing \end{bmatrix}}_{C_{ss}} x \end{aligned} \tag{3.2}$$

where

$$\dot{\psi} = \begin{cases} a(t-t_0), & t_0 < t < t_0 + t_a \\ at_a, & t_0 + t_a \leq t < \infty \end{cases}$$

The same with the open-loop system, the desired closed loop system is a LTV system in accelerating (transient) period, and then becomes a LTI system in steady-state period.

3.2 Analysis of the desired closed loop system

In this section, study of the desired closed loop system in Eq.3.2 is conducted, including its dynamic behaviors with respect to the choice of system parameters, and its stability, especially in transient period. Also, the physical sense of the system is included in the discussion. Concepts in rotordynamics, such as vibration modes and critical speed of rotor are introduced.

3.2.1 Stability analysis

Lyapunov direct method

A general interpretation of Lyapunov direct method, which applicable to both LTV system and LTI system is given by

Theorem 3.1 (Uniform exponential stability of linear time-varying system[5])**.** *The time varying linear dynamic system*

$$x^{\Delta}(t) = A(t)x(t), \qquad x(t_0) = x_0, \qquad t_0 \in \mathbb{T}$$

is uniformly exponentially stable if there exists a symmetric matrix $P(t) \in C_{rl}^{l}(\mathbb{T}, \mathbb{R}^{n\times n})$ *such that for all* $t \in \mathbb{T}$

1. $\eta I \leq P(t) \leq \rho I$
2. $A^{\top}(t)P(t) + (I + \mu(t)A^{\top}(t))(P^{\Delta}(t) + P(t)A(t) + \mu(t)P^{\Delta}(t)A(t)) \leq -\gamma I$, *where* $\gamma, \rho, \eta \in \mathbb{R}^{+}$ *and* $\frac{-\gamma}{\rho} \in \Re^{+}$.

Let $\mathbb{T} = \mathbb{R}$, and P be a constant matrix, then we have the following

- $x^{\Delta}(t) = \dot{x}$
- $\mu(t) = 0$
- $P^{\Delta}(t) = \dot{P} = 0$

The stability criteria become:

If

1. P is a positive definite matrix
2. $A^{\top}(t)P + PA(t)$ remains negative definite for all $t \in \mathbb{R}$.

the time varying linear dynamic system

$$\dot{x}(t) = A(t)x(t), \qquad x(t_0) = x_0, \qquad t_0 \in \mathbb{T}$$

is uniformly exponentially stable

Stability for a stabilized AMB system

Let the positive definite matrix P be solved from

$$A_{cl,ss}^{\top}(\dot{\psi}(t_0))P + PA_{cl,ss}(\dot{\psi}(t_0)) = -Q$$

where Q is a chosen positive definite matrix. It can be shown that $A_{cl,ss}^{\top}(\dot{\psi})P + PA_{cl,ss}(\dot{\psi})$ remains negative definite for $\forall t \in [t_0, \infty)$ when $\zeta^{con}\omega_n^{con}$ is sufficiently large. Therefore, by Theorem 3.1, the stabilized AMB system

$$\dot{x} = A_{cl,ss}(\dot{\psi})x$$

where

$$\dot{\psi} = \begin{cases} a(t - t_0), & t_0 < t < t_0 + t_a \\ at_a, & t_0 + t_a \leq t < \infty \end{cases}$$

is uniformly exponentially stable (asymptotically stable) about its equilibrium if $\zeta^{con}\omega_n^{con}$ is sufficiently large.

Numerical validation

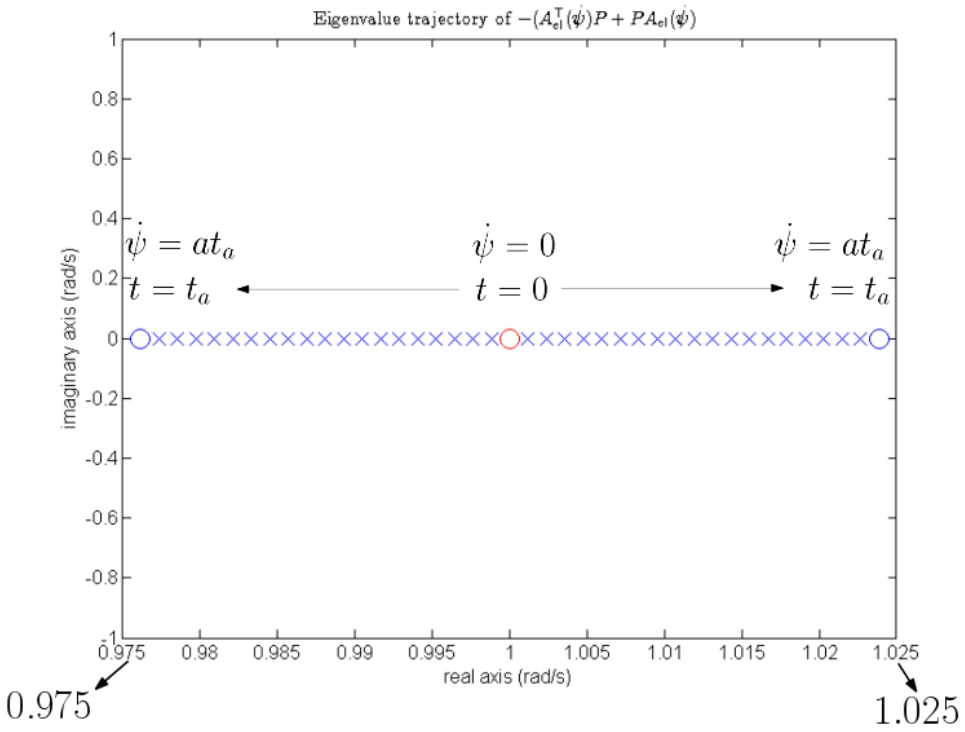

Figure 3.1: $\omega_n^{con} = 1000$ RPM, $\zeta^{con} = 0.5$, $Q = \text{eye}(4,4)$, $at_a = 10$K RPM

Model data is given by Table B.1. In Fig.3.1, a situation where ω_n^{con} is sufficient (1000 RPM) is shown. Even though the rotor accelerates to 10K RPM, stability of the stabilized system can still be guaranteed by Lyapunov theory. In Fig.3.2, a situation where ω_n^{con} is not sufficient (100 RPM) is shown. The sufficient condition described by Lyapunov theory is broke. Stability of the stabilized system can't be guaranteed.

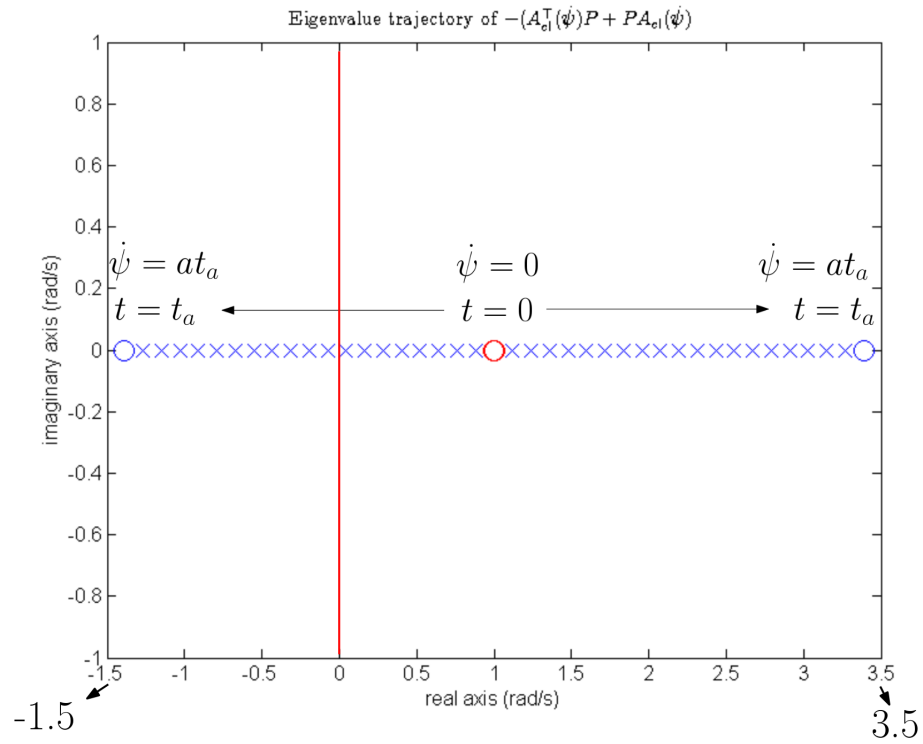

Figure 3.2: $\omega_n^{con} = 100$ RPM, $\varsigma^{con} = 0.5$, $Q = \text{eye}(4,4)$, $at_a = 10$K RPM

3.2.2 Vibration modes

Vibration mode indicates the shapes a structure vibrates in. There are two vibration modes for a rigid rotor. The *cylindrical mode*, which looks like a jumprope tracing the outline of a cylinder, is associated with the variables (X, Y) in Eq.3.1. The *conical mode*, which looks like a rod with its center fixed and its two ends tracing two circles, is associated with the variables (α, β) in Eq.3.1. Note that cylindrical mode and conical mode are decoupled in the desired closed loop system.

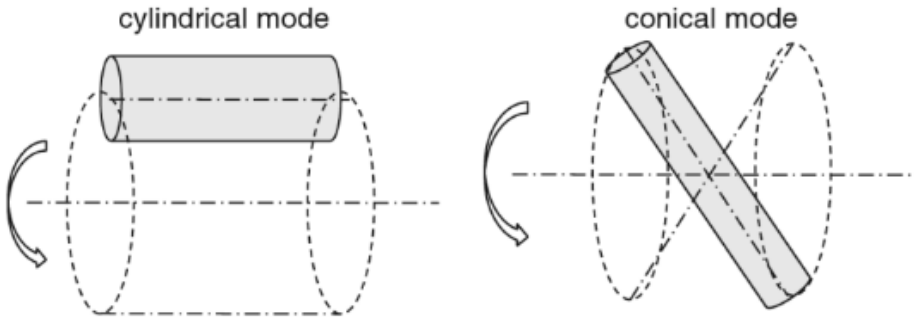

Figure 3.3: Cylindrical mode and conical mode of a rigid rotor [11]

In the context of *rotordynamics*, vibration of a rotor is also call *whirling*. If the whirling is in the same direction as the spinning of rotor, this kind of whirling is called *forward whirling*. If the whirling is in the opposite direction to the spinning of rotor, this kind of whirling is called *backward whirling*. Both cylindrical mode and conical mode have forward and backward whirling.

3.2.3 Varying operating speed analysis

Speed-dependent eigenvalues

In varying operating speed analysis, rotor is assumed to be in steady-state at each operating speed, that is, $\dot{\psi}$ is always a constant. The system becomes LTI in both accelerating period and steady-state period. Thus, techniques for analyzing LTI system, such as eigenvalue analysis can be carried out for the system.

When the rotor doesn't spin, $\dot{\psi} = 0$. The state matrix has four pairs of eigenvalues. The two pairs corresponding to cylindrical mode are given by

$$s_{1,2}^{cyl} = s_{3,4}^{cyl} = -\zeta^{cyl}\omega_n^{cyl} \pm \omega_n^{cyl}\sqrt{1-(\zeta^{cyl})^2}i \tag{3.3}$$

The two pairs corresponding to conical mode are given by

$$s_{1,2}^{nut} = s_{3,4}^{pre} = -\zeta^{con}\omega_n^{con} \pm \omega_n^{con}\sqrt{1-(\zeta^{con})^2}i \tag{3.4}$$

When the rotor spins, $\dot{\psi} \neq 0$, the two pairs of eigenvalues corresponding to conical mode split from its original location in *s-plane*. The pair $s_{1,2}^{nut}$, which is corresponding to the nutation mode (the forward mode of conical mode), moves to the left of its original location with a increase in its corresponding natural frequency. The pair $s_{3,4}^{pre}$, which is corresponding to the precession mode (the backward mode of conical mode), moves to the right of its original location with a decrease of its corresponding natural frequency. $s_{1,2}^{nut}$ can only be excited under forward mode excitation, while $s_{3,4}^{pre}$ can only be excited under forward mode excitation. In summary, the eigenvalues corresponding to conical mode are speed-dependent.

Eigenvalue trajectory and Campbell diagram

To better visualize the behaviors of these two pairs of eigenvalues corresponding to conical mode, eigenvalues trajectory and Campbell diagram can be used. Let the system parameters of conical mode be given by Table 3.2.3. Fig. 3.4 shows the eigenvalue trajectory. Fig. 3.5 and Fig. 3.6 show the Campbell diagrams of damped natural frequency and damping ratio respectively.

symbol	value	units
ω_n^{con}	50	rad/s
ζ^{con}	0.707	N/A

Table 3.1: System parameters for conical mode

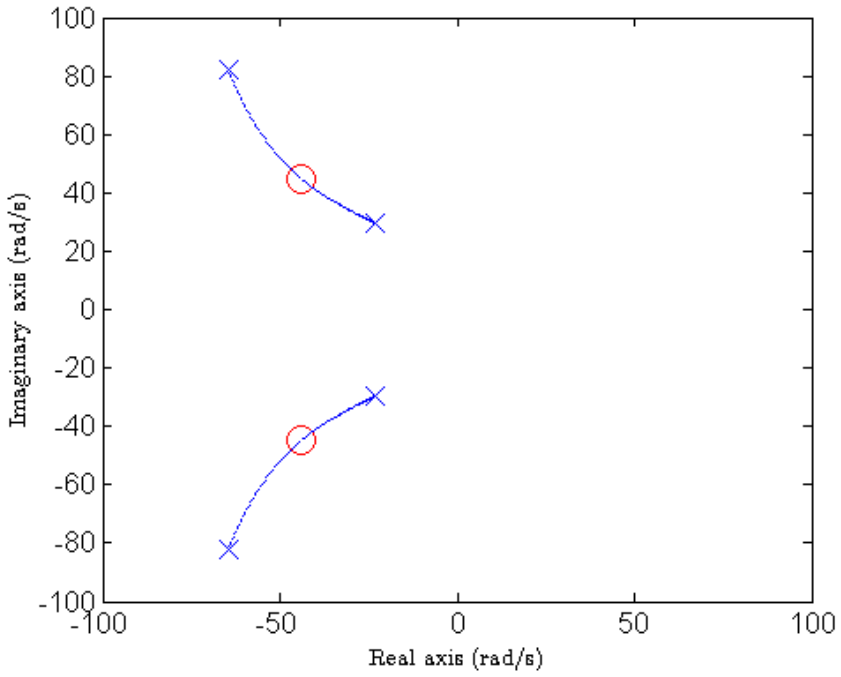

Figure 3.4: Eigenvalue trajectory of the speed-dependent eigenvalues (red circle: $\dot{\psi} = 0$ RPM; blue cross: $\dot{\psi} = 1000$ RPM)

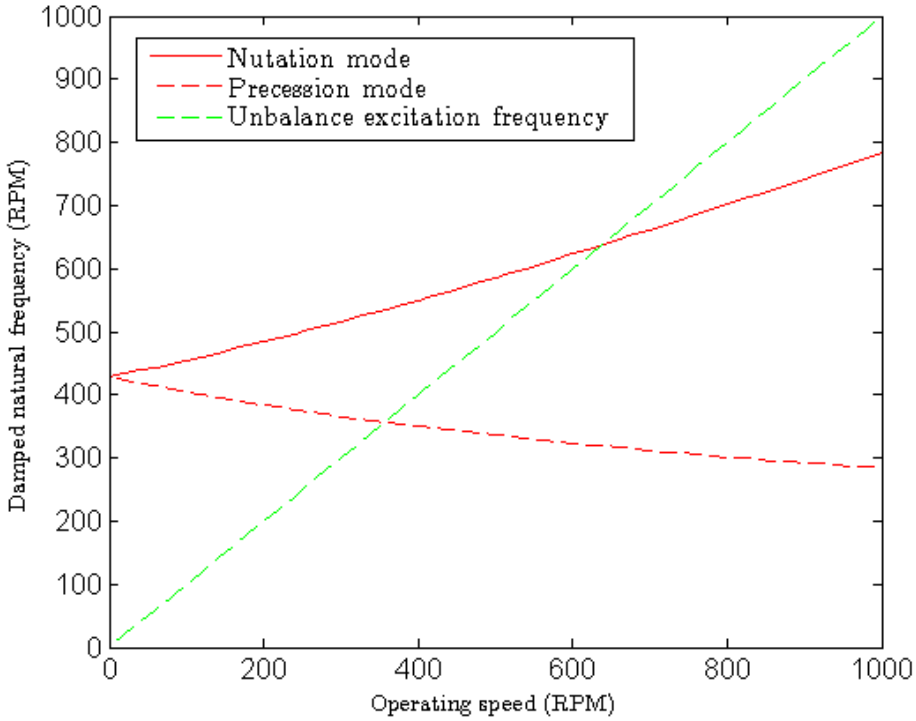

Figure 3.5: The speed-dependent damped natural frequencies of nutation and precession

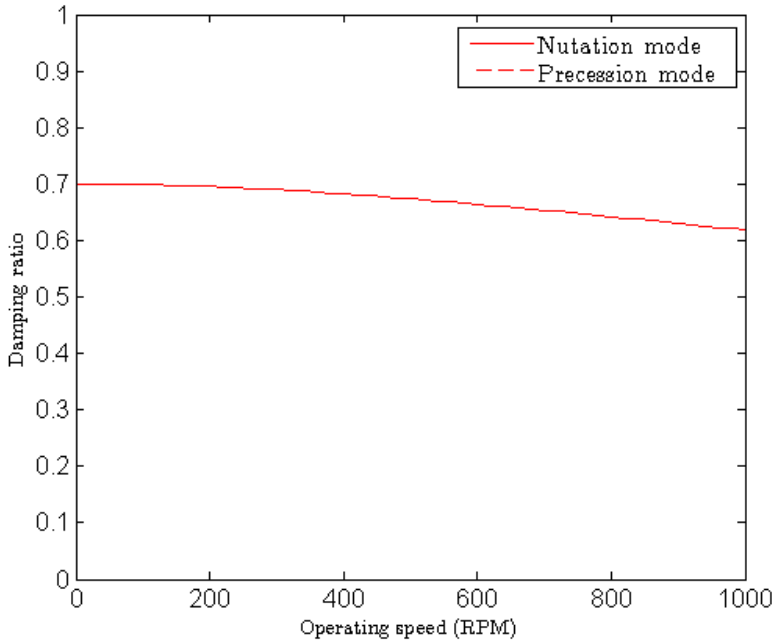

Figure 3.6: The speed-dependent damping ratios of nutation and precession

In Fig.3.4, the pair of eigenvalues corresponding to precession mode travels to a location very close to the imaginary axis in high operating speed. This can be a potential issue deteriorating the system performance once precession mode is excited.

In the Campbell diagram Fig.3.5, the green line represents the excitation frequency of unbalance excitation. According to *American Petroleum Institute (API)* [12], the operating speed corresponding to the location where the green line crosses the red line is called *critical speed* for conical mode *if* there is a peak vibration response. In this example, the damping ratio stays in a good condition (0.6-0.7) for the whole operating speed range, so there will not be any vibration peak at this crossing point. Consequently, this point cannot be called critical speed.

The strength of gyroscopic effects can be distinguish by how fast the two pairs of eigenvalues splitting from each other in eigenvalue trajectory, and how fast the damped natural frequency and damping ratio change in Campbell diagrams.

3.2.4 Transient response

In many applications, static load will be acted on the rotor, which makes it important to study the static load response. Also, every rotor has a certain amount of unbalance due to manufacturing error, the investigation of unbalance response is important. Therefore, two kinds of transient response are investigated in the section, which are transient static load response and transient unbalance response.

In transient response, the eigenvalue analysis is no longer valid. It will be useful to have analytical solution for the response. But it is also hard to draw any conclusion from those complicated forms of solution. To better understand the dynamic performances, computer simulation is used. The model data of this thesis are consistently based on Table B.1, except I_P, which will be varying depending on the factor p; and m_u, which will be varying depending on the unbalance ratio c_u. The reason for using different values for these two

model parameters, is to investigate more situations and make the work in this thesis also applicable for other AMB systems.

In simulation, rotor accelerates from 0 RPM to 5000 RPM in 10 seconds.

Transient unbalance response

The effect of natural frequency and damping ratio: The rotor is assumed to have 0.02 % unbalance, which is a small ratio representing the manufacturing error in every rotor. The factor p is chosen to be 0.5, so the effect of gyroscopic terms is obvious enough to be seen.

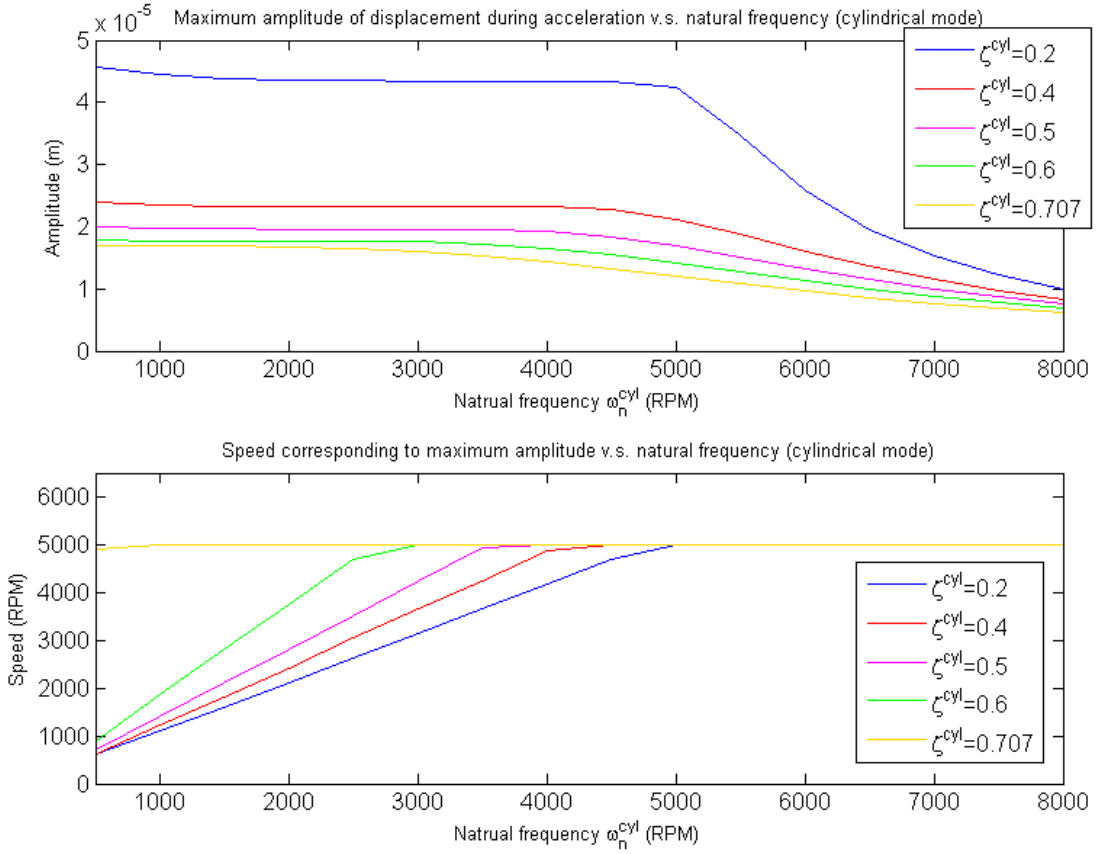

Figure 3.7: Maximum response amplitude and the corresponding rotor speed in transient unbalance response for different ω_n^{cyl} and ζ^{cyl}

The upper plot of Fig.3.7 shows that ω_n^{cyl} has a little effect in reducing the maximum amplitude during acceleration, especially when ζ^{cyl} is larger than 0.4. Taking the situation where $\zeta^{cyl} = 0.5$ as an example, when ω_n^{cyl} increases from 1000 RPM to 5000 RPM, the maximum amplitude only reduces 10 %.

In the lower plot of Fig.3.7, if we just look at one of the lines, let's say the line corresponding to $\zeta^{cyl} = 0.2$. The rotor speed in y axis equal to 5000 RPM means that this choice of natural frequency gets rid of resonance in the speed range. The minimum ω_n^{cyl} to get rid of resonance in the speed range decreases with the increase of ζ^{cyl}. When $\zeta^{cyl} = 0.707$, there is no resonance for any choice of ω_n^{cyl}.

If we just look at one value of ω_n^{cyl}, let's say $\omega_n^{cyl} = 2000$ RPM. In the lower plot, with the increase of ζ^{cyl}, the resonance speed increases. This is different from what bode plot for an underdamped second order system shows. In the bode plot, with the increase of damping, the resonance speed decreases. The reason is, in bode plot, the amplitude of excitation doesn't have the speed-squared characteristic as in the one of unbalance excitation.

In choosing desired system parameters for cylindrical mode, firstly, we want the maximum amplitude to be less than 2e-5 meters, which is less than 10 % of the air gap in our model. This requirement will be satisfied as long as ζ^{cyl} is chosen to be larger than 0.4. Secondly, we want ω_n^{cyl} to be small. Because a high ω_n^{cyl} introduces more high frequency noise into the system, and the *bending modes* of rotor are more likely to occur. However, ω_n^{cyl} can not be too low either, or the step response will be very slow.

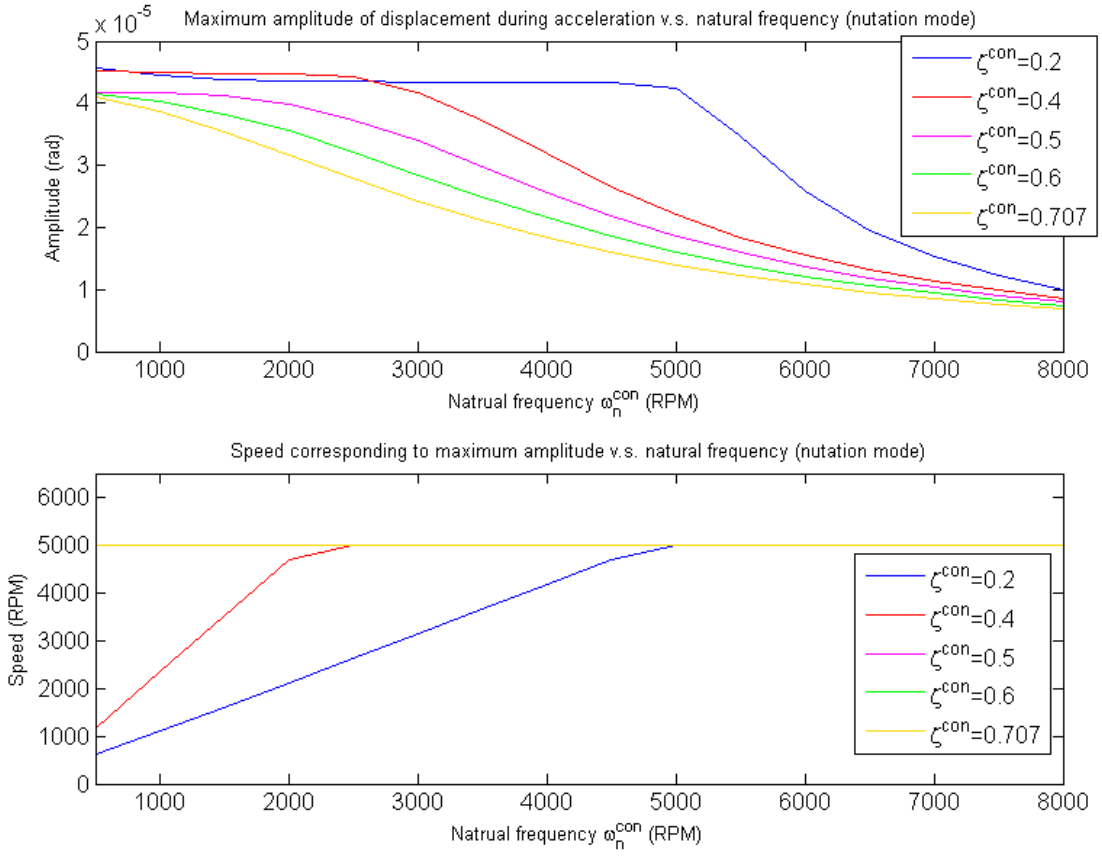

Figure 3.8: Maximum response amplitude and the corresponding rotor speed in transient unbalance response for different ω_n^{con} and ζ^{con}

The upper plot of Fig.3.8 shows that ω_n^{con} has a evident effect in reducing the maximum amplitude in transient unbalance response. Taking the situation where $\zeta^{con} = 0.5$ as an example, when ω_n^{con} increases from 1000 RPM to 5000 RPM, the maximum amplitude reduces 50 %.

The lower plot of Fig.3.8 shows that when ζ^{con} is greater than 0.4, resonance disappears for all choice of ω_n^{con}. This value of damping ratio is much lower than the one in cylindrical mode. The reason is that the gyroscopic terms stiffen the natural frequency in conical mode with the increase of rotor speed. Thus the frequency ratio could never reaches one during acceleration.

In choosing desired system parameters for conical mode, firstly, we want the maximum amplitude of rotational displacement be less than 3e-5 radians. Along with the requirement for maximum amplitude of translational displacement, the maximum amplitude of displacement in bearing planes will be less than 2.5e-5 meters, which is 10 % of the air gap. Secondly, we want ω_n^{con} be low to avoid high frequency noise. But the settling time in step response can not be too slow.

The effect of gyroscopic dynamics: Because gyroscopic effects only act on conical mode. Only the response of conical mode need to be studied.

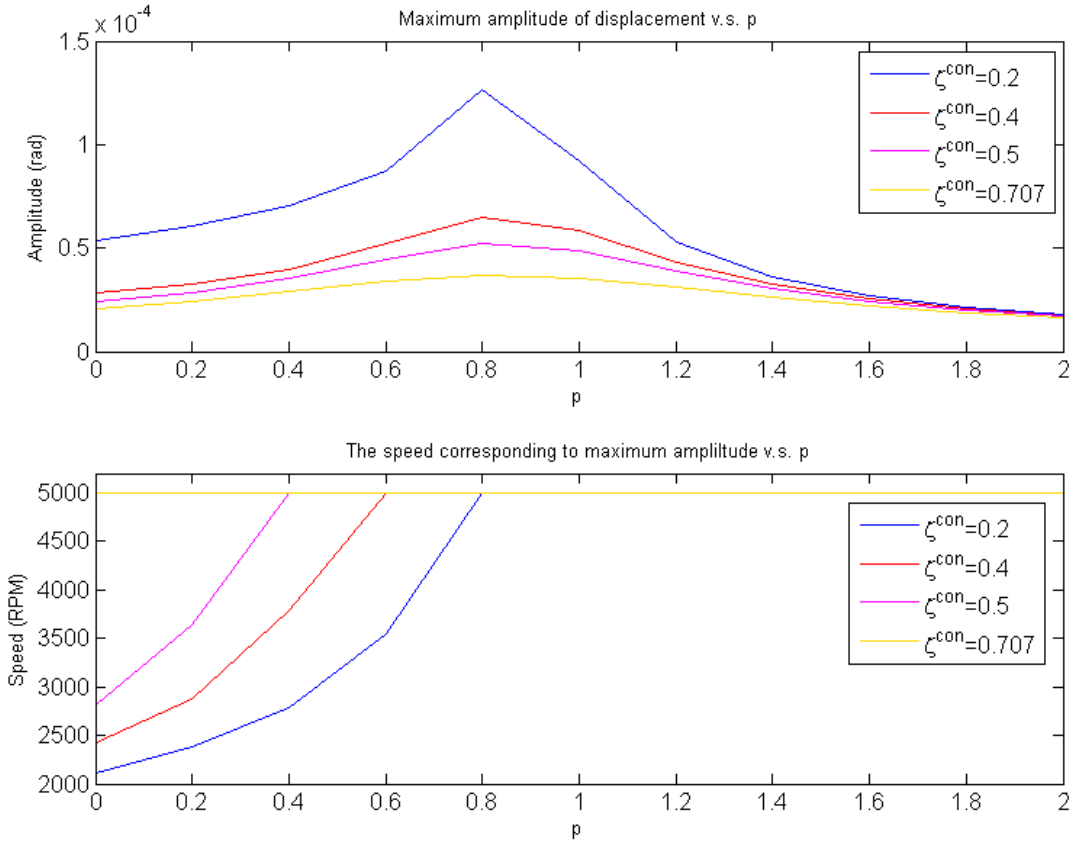

Figure 3.9: Maximum response amplitude and the corresponding rotor speed in acceleration v.s p (ω_n^{con} less than the upper bound of the speed range)

In Fig.3.9, ω_n^{con} is chosen to be less than the upper bound of the speed range. The upper plot of Fig.3.9 shows that when p is smaller than 0.8, with the increase of p, the

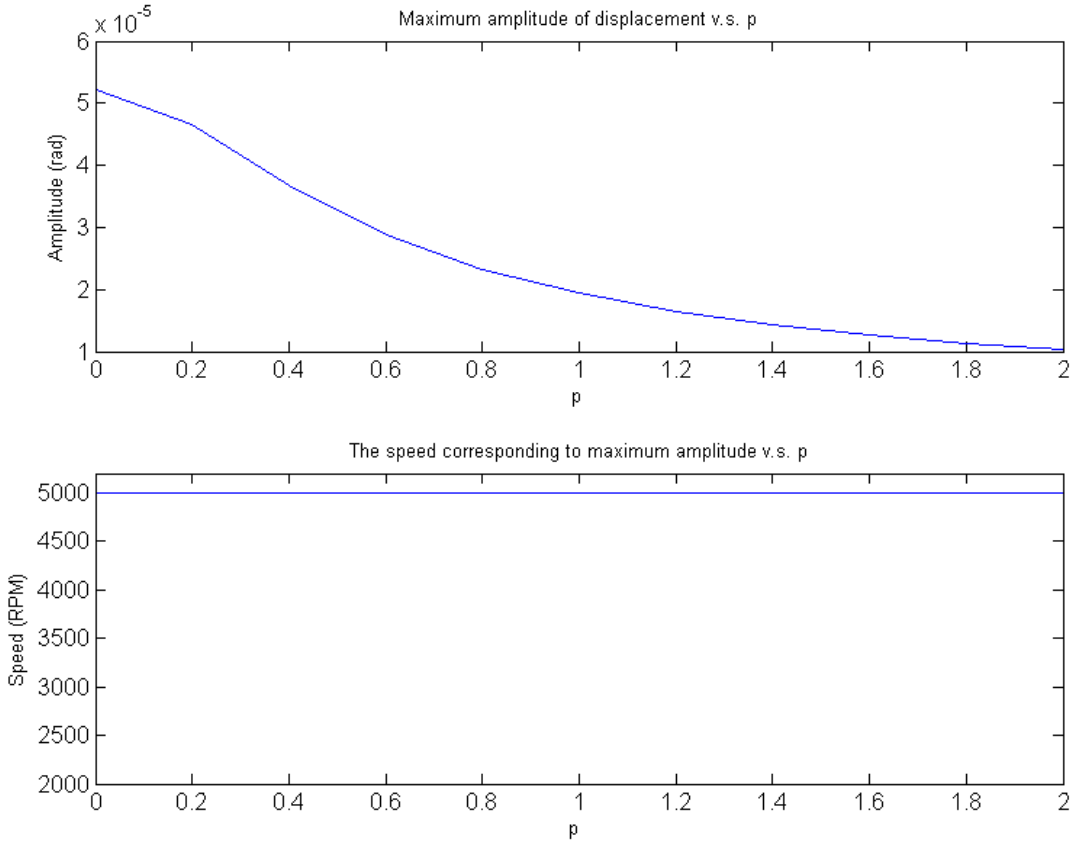

Figure 3.10: Maximum response amplitude and the corresponding rotor speed in acceleration v.s p (ω_n^{con} larger than the upper bound of the speed range)

maximum amplitude also increases. When p is larger than 0.8, with the increase of p, the maximum amplitude decreases. The effect is more obvious when ζ^{con} is smaller. The lower plot of Fig.3.9 shows that, for different choices of ζ^{con}, there are different values of p where resonance totally disappears in the speed range.

In Fig.3.10, ω_n^{con} is chosen to be larger than the upper bound of the speed range. The upper plot of Fig.3.10 shows that the maximum amplitude decreases with the increase in p no matter what is the choice of ζ^{con}. The lower plot of Fig.3.10 shows that there will be no resonance in the speed range no matter what is the choice of ζ^{con}.

In choosing desired system parameters, we tend to choose ω_n^{con} less than the upper bound of speed range. Therefore, our decision is based on Fig.3.9. Now suppose we can control

the value of p, which is impossible for conventional rotor-bearing system, but is possible for AMB systems. If p is in the range of 0.6 to 0.8, attenuating p into the range of 0.1 to 0.3 helps reducing the maximum amplitude. If p is in the range of 0.8 to 1.2, attenuating p into the range of 0.1 to 0.3 may cost too much control power. If p is larger than 1.2, there is no need to attenuate p from the point of reducing maximum amplitude.

Transient static load response

Static force with amplitude of 5 N, and static torque with amplitude of 0.75 N·m are acted periodically on the translational variable X and the rotational variable α.

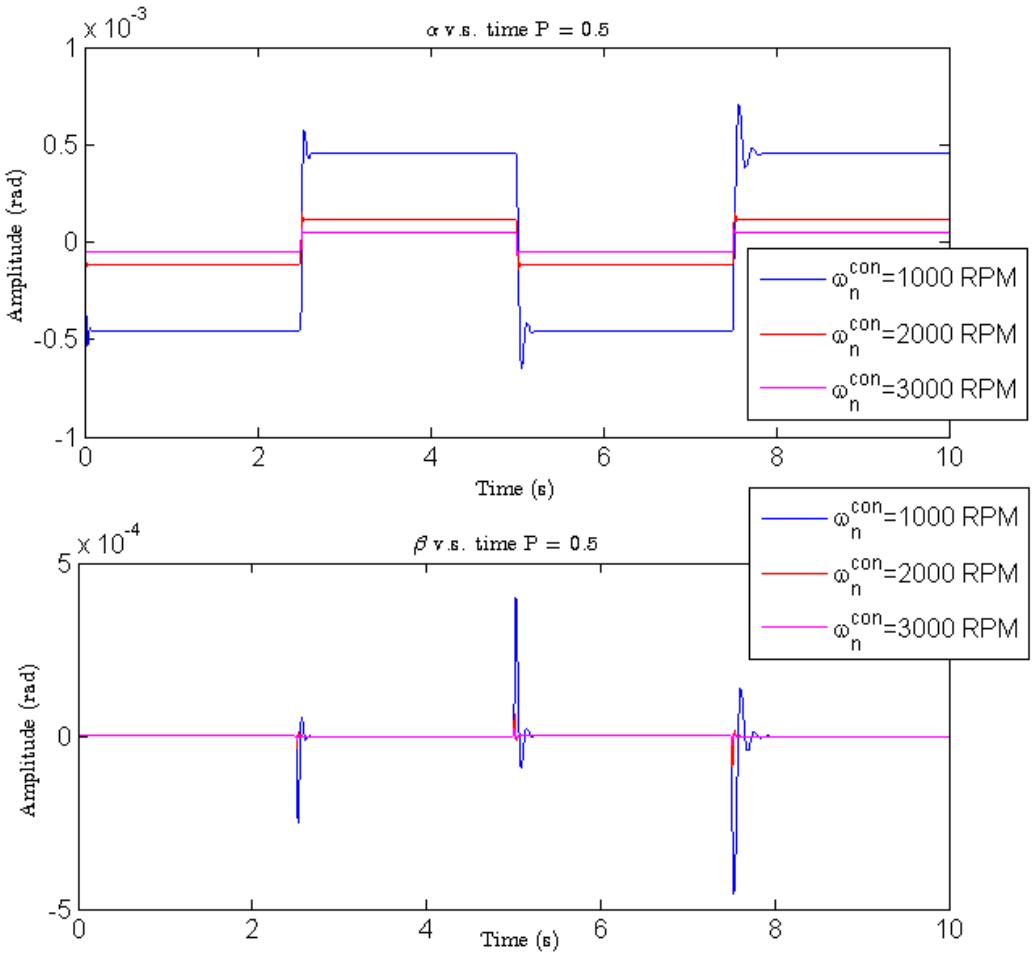

Figure 3.11: Transient static load response during acceleration for different ω_n^{con}

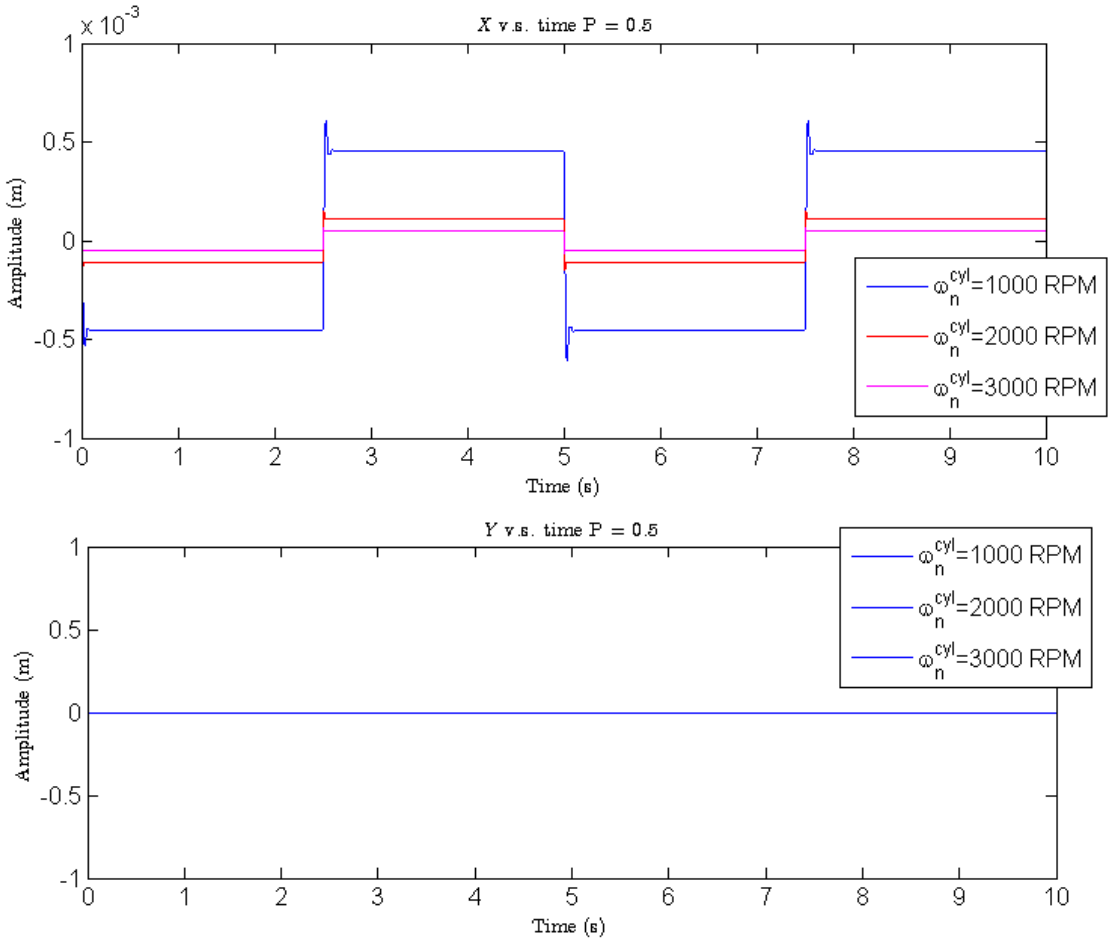

Figure 3.12: Transient static load response during acceleration for different ω_n^{cyl}

The effect of natural frequency: Fig.3.11 shows that, for conical mode, the amplitude in transient static load response only depends on ω_n^{con} but not ω_n^{nut} nor ω_n^{pre}. With the increase of speed, the coupling effects of two rotational variables become stronger, which results in a larger impulse disturbance in β, as well as a larger percentage overshoot and a longer settling time in α.

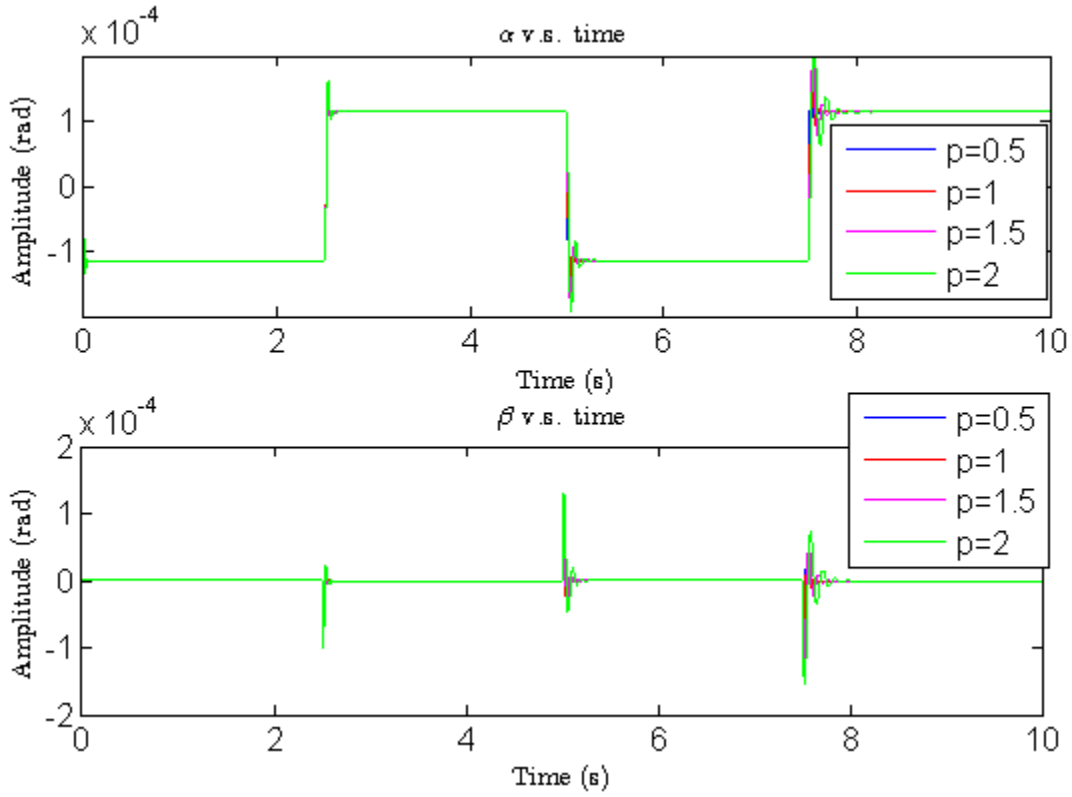

Figure 3.13: Static load response in acceleration for different P

The effect of gyroscopic dynamics: With the increase of p, the coupling effects of two rotational variables become stronger, which results in a larger impulse disturbance in β, as well as a larger percentage overshoot and a longer settling time in α.

Therefore, from the point of static load response, the natural frequency is desired to be large in order to obtain a low value of static deflection. The factor p is desired to be small to reduce the coupling effects between two rotational variables.

The desired system parameters

Based on the above analysis, the following desired system parameters are selected for the stabilizing controller design for the AMB system described by Table B.1.

Note that ω_n^{cyl} and ω_n^{con} are chosen to be smaller than the maximum operating speed, in this case, 5000 RPM, to avoid the generation of high frequency noise and the occur of

symbol	value	unit
ζ^{con}	0.5	N/A
ζ^{cyl}	0.4	N/A
ω_n^{cyl}	1200	RPM
ω_n^{con}	3500	RPM

Table 3.2: Desired system parameters for stabilizing controller design

bending modes of rotor. The choice of ζ^{con} and ζ^{cyl} are adequate to limit the vibration peak during acceleration.

3.3 Comparison study between local PD control and centralized PD control

In this section, how to use a PD-typed controller to obtain the desired closed loop system is explored. In all the previous work in RML ([3], [10] and [8]), the stabilizing controller is chosen to be a local PD controller. Because the rotor model in these works is a simplified planar model, the local PD controller doesn't seem to have any issue. However, if the rotor is modeled in three dimensional, poor dynamic performance is shown by using local PD controller. Therefore, a centralized PD controller is needed to obtain a better dynamic performance.

3.3.1 Local PD controller design

Local (decentralized) PD control is the easiest way to stabilize an AMB system. In applying local PD control, the conical mode vibration is ignored. Therefore, the motion of rotor can be treated as the motions of two planar rigid rotors in each bearing plane. The control task is *decentralized* into two unrelated tasks.

The control law is given by

$$i = -K_p q_s - K_d \dot{q}_s \tag{3.5}$$

where q_s is the variables of rotor in sensor coordinate system;

$$K_p = \begin{bmatrix} k_{p1} & 0 & 0 & 0 \\ 0 & k_{p2} & 0 & 0 \\ 0 & 0 & k_{p1} & 0 \\ 0 & 0 & 0 & k_{p2} \end{bmatrix} \tag{3.6}$$

$$K_d = \begin{bmatrix} k_{d1} & 0 & 0 & 0 \\ 0 & k_{d2} & 0 & 0 \\ 0 & 0 & k_{d1} & 0 \\ 0 & 0 & 0 & k_{d2} \end{bmatrix} \tag{3.7}$$

The closed loop system can be written as

$$M\ddot{q} + G\dot{q} + BK_sB^\top q = BK_i(-K_pq_s - K_d\dot{q_s}) \tag{3.8}$$

Using the coordinate transformation $q_s = Cq$ to transform the variables from sensor coordinates to rotor coordinates, the closed loop system becomes

$$M\ddot{q} + G(\dot{\psi})\dot{q} + BK_sB^\top q = BK_i(-K_pCq - K_dC\dot{q})$$

$$M\ddot{q} + (G(\dot{\psi}) + BK_iK_dC)\dot{q} + (BK_sB^\top + BK_iK_pC)q = 0$$

$$\begin{bmatrix} I_T & 0 & 0 & 0 \\ 0 & m & 0 & 0 \\ 0 & 0 & I_T & 0 \\ 0 & 0 & 0 & m \end{bmatrix} \ddot{q} + \begin{bmatrix} L_BL_Sk_i(k_{d1}+k_{d2}) & L_Bk_i(k_{d1}-k_{d2}) & -I_P\dot{\psi} & 0 \\ L_Sk_i(k_{d1}-k_{d2}) & k_i(k_{d1}+k_{d2}) & 0 & 0 \\ I_P\dot{\psi} & 0 & L_BL_Sk_i(k_{d1}+k_{d2}) & L_Bk_i(k_{d2}-k_{d1}) \\ 0 & 0 & L_Sk_i(k_{d2}-k_{d1}) & k_i(k_{d2}+k_{d1}) \end{bmatrix} \dot{q} \tag{3.9}$$

$$+ \begin{bmatrix} 2k_sL_B^2+L_BL_Sk_i(k_{p1}+k_{p2}) & L_Bk_i(k_{p1}-k_{p2}) & 0 & 0 \\ L_Sk_i(k_{p1}-k_{p2}) & 2k_s+k_i(k_{p1}+k_{p2}) & 0 & 0 \\ 0 & 0 & 2k_sL_B^2+L_BL_Sk_i(k_{p2}+k_{p1}) & L_Bk_i(k_{p2}-k_{p1}) \\ 0 & 0 & L_Sk_i(k_{p2}-k_{p1}) & 2k_s+k_i(k_{p1}+k_{p2}) \end{bmatrix} q = 0$$

Because the speed-dependent gyroscopic terms, two variables associated with conical mode are coupled. Furthermore, in Eq.3.9, if $k_{d1} \neq k_{d2}$ and $k_{p1} \neq k_{p2}$, the variables associated with cylindrical mode will couple with the variables associated with conical mode, and consequently become speed-dependent too, which is not what we want. To avoid the coupling

of cylindrical mode and conical mode, it is natural to choose

$$k_{p1} = k_{p2} = k_p$$

$$k_{d1} = k_{d2} = k_d$$

The closed loop system becomes:

$$\begin{bmatrix} I_T & 0 & 0 & 0 \\ 0 & m & 0 & 0 \\ 0 & 0 & I_T & 0 \\ 0 & 0 & 0 & m \end{bmatrix} \ddot{q} + \begin{bmatrix} 2L_B L_S k_i k_d & 0 & -I_P\dot{\psi} & 0 \\ 0 & 2k_i k_d & 0 & 0 \\ I_P\dot{\psi} & 0 & 2L_B L_S k_i k_d & 0 \\ 0 & 0 & 0 & 2k_i k_d \end{bmatrix} \dot{q}$$
$$+ \begin{bmatrix} 2k_s L_B^2 + 2L_B L_S k_i k_p & 0 & 0 & 0 \\ 0 & 2k_s + 2k_i k_p & 0 & 0 \\ 0 & 0 & 2k_s L_B^2 + 2L_B L_S k_i k_p & 0 \\ 0 & 0 & 0 & 2k_s + 2k_i k_p \end{bmatrix} q = 0 \tag{3.10}$$

Let ζ^{cyl} and ω_n^{cyl} be the desired closed loop system parameters for cylindrical mode. We have

$$\frac{2k_d k_i}{m} = 2\zeta^{cyl}\omega_n^{cyl} \tag{3.11}$$

$$\frac{2k_s + 2k_i k_p}{m} = (\omega_n^{cyl})^2 \tag{3.12}$$

Therefore, the feedback gains are given by

$$k_d = \frac{\zeta^{cyl}\omega_n^{cyl} m}{k_i} \tag{3.13}$$

$$k_p = \frac{(\omega_n^{cyl})^2 m - 2k_s}{2k_i} \tag{3.14}$$

From the point of stability in cylindrical mode, k_p need to satisfy

$$k_p > -\frac{k_s}{k_i} \tag{3.15}$$

The closed loop system parameters for conical mode corresponding to the choice of k_p and k_d are given by

$$\begin{aligned} 2\zeta^{con}\omega_n^{con} &= \frac{2k_d k_i L_B L_S}{I_T} \\ &= \left(\frac{L_B L_S m}{I_T}\right) 2\zeta^{cyl}\omega_n^{cyl} \end{aligned} \tag{3.16}$$

$$\begin{aligned} (\omega_n^{con})^2 &= \frac{2k_s L_B^2 + 2L_B L_S k_i k_p}{I_T} \\ &= \left(\frac{L_B L_S m}{I_T}\right)(\omega_n^{cyl})^2 + \frac{2k_s L_B^2 - 2k_s L_B L_S}{I_T} \end{aligned} \tag{3.17}$$

From the point of stability in conical mode, $(\omega_n^{con})^2$ need to be a positive number, then we have

$$\begin{aligned} \left(\frac{L_B L_S m}{I_T}\right)\left(\frac{2k_s + 2k_i k_p}{m}\right) + \frac{2k_s L_B^2 - 2k_s L_B L_S}{I_T} > 0 \\ k_p > \frac{-L_B^2 k_s}{L_B L_S k_i} \end{aligned} \tag{3.18}$$

The closed loop system parameters for conical mode are given by

$$\omega_n^{con} = \sqrt{\left(\frac{L_B L_S m}{I_T}\right)(\omega_n^{cyl})^2 + \frac{2k_s L_B^2 - 2k_s L_B L_S}{I_T}} \tag{3.19}$$

$$\zeta^{con} = \sqrt{\frac{(L_b L_s m)^2 (\omega_n^{cyl})^2}{(L_b L_s m(\omega_n^{cyl})^2 + (2k_s L_B^2 - 2k_s L_B L_S))I_T}}\zeta^{cyl} \tag{3.20}$$

Limitations of local PD controller

System parameters for conical mode and cylindrical mode are dependent: From Eq.3.19 and Eq.3.19, once ω_n^{cyl} and ζ^{cyl} are chosen, ω_n^{con} and ζ^{con} are decided. There is no freedom to design conical mode and cylindrical mode independently. Moreover, the dependency always results in a high value for ζ^{con} and ω_n^{cyl}, but a merely enough value for ζ^{cyl} and ω_n^{con}. Therefore, the distribution of control effort is unbalanced.

Possible instability issue in conical mode: According to Eq.3.15 and Eq.3.18, for the AMB systems with $L_B > L_S$, the stability requirement for conical mode is more stringent than the stability requirement for cylindrical mode. If one design the feedback gains only based on cylindrical mode, when conical mode vibration is excited, the rotor can become unstable. Therefore, using local PD control, k_p need to be a large number in case of the instability issue.

3.3.2 Centralized PD controller design

Unlike local PD controller only taking part of the model (cylindrical mode) into consideration, the design of centralized PD controller is model-orientated with a full utilization of the system model. Therefore, the control is able to go into the rotor coordinates effectively.

Define a controller input operator as

$$\begin{aligned} T_{in} &= (C)^{-1} \\ &= \begin{bmatrix} \frac{1}{2L_s} & \frac{-1}{2L_s} & 0 & 0 \\ \frac{1}{2} & \frac{1}{2} & 0 & 0 \\ 0 & 0 & \frac{-1}{2L_s} & \frac{1}{2L_s} \\ 0 & 0 & \frac{1}{2} & \frac{1}{2} \end{bmatrix} \end{aligned} \tag{3.21}$$

which is actually a coordinate transformation matrix transforming the variables from sensor coordinates back to rotor coordinates.

Define a controller output operator as

$$\begin{aligned} T_{out} &= (BK_i)^{-1} \\ &= K_i^{-1}B^{-1} \\ &= \begin{bmatrix} \frac{1}{2k_iL_b} & \frac{1}{2k_i} & 0 & 0 \\ -\frac{1}{2k_iL_b} & \frac{1}{2k_i} & 0 & 0 \\ 0 & 0 & -\frac{1}{2k_iL_b} & \frac{1}{2k_i} \\ 0 & 0 & \frac{1}{2k_iL_b} & \frac{1}{2k_i} \end{bmatrix} \end{aligned} \tag{3.22}$$

which resolves the coupling effects of input path BK_i.

The control law is given by

$$
\begin{aligned}
i &= -T_{out}K_pT_{in}q_s - T_{out}K_dT_{in}\dot{q}_s \\
&= \begin{bmatrix} \frac{k_{p1}}{2L_Bk_i} & \frac{k_{p2}}{2k_i} & 0 & 0 \\ -\frac{k_{p1}}{2L_Bk_i} & \frac{k_{p2}}{2k_i} & 0 & 0 \\ 0 & 0 & -\frac{k_{p1}}{2L_Bk_i} & \frac{k_{p2}}{2k_i} \\ 0 & 0 & \frac{k_{p1}}{2L_Bk_i} & \frac{k_{p2}}{2k_i} \end{bmatrix} \begin{bmatrix} \alpha \\ X \\ \beta \\ Y \end{bmatrix} + \begin{bmatrix} \frac{k_{d1}}{2L_Bk_i} & \frac{k_{d2}}{2k_i} & 0 & 0 \\ -\frac{k_{d1}}{2L_Bk_i} & \frac{k_{d2}}{2k_i} & 0 & 0 \\ 0 & 0 & -\frac{k_{d1}}{2L_Bk_i} & \frac{k_{d2}}{2k_i} \\ 0 & 0 & \frac{k_{d1}}{2L_Bk_i} & \frac{k_{d2}}{2k_i} \end{bmatrix} \begin{bmatrix} \dot{\alpha} \\ \dot{X} \\ \dot{\beta} \\ \dot{Y} \end{bmatrix}
\end{aligned} \tag{3.23}
$$

where

$$
K_d = \begin{bmatrix} k_{d1} & 0 & 0 & 0 \\ 0 & k_{d2} & 0 & 0 \\ 0 & 0 & k_{d1} & 0 \\ 0 & 0 & 0 & k_{d2} \end{bmatrix} \tag{3.24}
$$

$$
K_p = \begin{bmatrix} k_{p1} & 0 & 0 & 0 \\ 0 & k_{p2} & 0 & 0 \\ 0 & 0 & k_{p1} & 0 \\ 0 & 0 & 0 & k_{p2} \end{bmatrix} \tag{3.25}
$$

The closed loop system is given by

$$
\begin{aligned}
M\ddot{q} + G(\dot{\psi})\dot{q} + BK_sB^\top q &= BK_i i \\
M\ddot{q} + G(\dot{\psi})\dot{q} + BK_sB^\top q &= BK_i(-T_{out}K_pT_{in}q_s - T_{out}K_dT_{in}\dot{q}_s) \\
M\ddot{q} + G(\dot{\psi})\dot{q} + BK_sB^\top q &= -IK_pT_{in}q_s - IK_dT_{in}\dot{q}_s \\
M\ddot{q} + (G(\dot{\psi}) + K_d)\dot{q} + (BK_sB^\top + K_p)q &= 0 \\
\begin{bmatrix} I_T & 0 & 0 & 0 \\ 0 & m & 0 & 0 \\ 0 & 0 & I_T & 0 \\ 0 & 0 & 0 & m \end{bmatrix} \ddot{q} + \begin{bmatrix} k_{d1} & 0 & -I_P\dot{\psi} & 0 \\ 0 & k_{d2} & 0 & 0 \\ I_P\dot{\psi} & 0 & k_{d1} & 0 \\ 0 & 0 & 0 & k_{d2} \end{bmatrix} \dot{q} + \begin{bmatrix} 2k_sL_B^2+k_{p1} & 0 & 0 & 0 \\ 0 & 2k_s+k_{p2} & 0 & 0 \\ 0 & 0 & 2k_sL_B^2+k_{p1} & 0 \\ 0 & 0 & 0 & 2k_s+k_{p2} \end{bmatrix} q &= 0
\end{aligned} \tag{3.26}
$$

With the help of T_{in} and T_{out}, the feedback gains are directly acted on the state without any scaling and coupling. Also, the design of closed loop parameters for conical mode and cylindrical mode can be performed separately, which is an unique features compared to local PD controller.

From the point of stability, k_{p1} and k_{p2} need to satisfy

$$k_{p1} > -2k_s L_B^2 \tag{3.27}$$

$$k_{p2} > -2k_s \tag{3.28}$$

With the chosen desired system parameters ζ^{cyl}, ω_n^{cyl}, ζ^{con} and ω_n^{con}, the feedback gains can be calculated by

$$k_{d1} = 2\zeta^{con}\omega_n^{con} I_T \tag{3.29}$$

$$k_{d2} = 2\zeta^{cyl}\omega_n^{cyl} m \tag{3.30}$$

$$k_{p1} = I_T(\omega_n^{con})^2 - 2k_s L_B^2 \tag{3.31}$$

$$k_{p2} = m(\omega_n^{cyl})^2 - 2k_s \tag{3.32}$$

In state variable description, the closed loop system can be written as

$$\begin{bmatrix} \dot{q} \\ \ddot{q} \end{bmatrix} = \begin{bmatrix} 0 & 0 & 0 & 0 & 1 & 0 & 0 & 0 \\ 0 & 0 & 0 & 0 & 0 & 1 & 0 & 0 \\ 0 & 0 & 0 & 0 & 0 & 0 & 1 & 0 \\ 0 & 0 & 0 & 0 & 0 & 0 & 0 & 1 \\ -\frac{2k_s L_B^2 + k_{p1}}{I_T} & 0 & 0 & 0 & -\frac{k_{d1}}{I_T} & 0 & \frac{I_P \dot{\psi}}{I_T} & 0 \\ 0 & -\frac{2k_s + k_{p2}}{m} & 0 & 0 & 0 & -\frac{k_{d2}}{m} & 0 & 0 \\ 0 & 0 & -\frac{2k_s L_B^2 + k_{p3}}{I_T} & 0 & -\frac{I_P \dot{\psi}}{I_T} & 0 & -\frac{k_{d3}}{I_T} & 0 \\ 0 & 0 & 0 & -\frac{2k_s + k_{p4}}{m} & 0 & 0 & 0 & -\frac{k_{d4}}{m} \end{bmatrix} \begin{bmatrix} q \\ \dot{q} \end{bmatrix} \tag{3.33}$$

3.3.3 Active gyroscopic attenuation

In Section 3.2.4, we argue that, from the point of unbalance response, attenuating p from the range of 0.3 to 0.8 to the range of 0.1 to 0.3 can reduce the maximum amplitude of displacement; from the point of static response, a smaller p yields a better performances. With conventional bearings, there is no way to influence p. Luckily, with AMBs, a speed-dependent feedback gain matrix can attenuate p into whatever value we want.

The control law is given by

$$i = -T_{out}K_pT_{in}q_s - T_{out}K_d(\dot{\psi})T_{in}\dot{q_s} \tag{3.34}$$

which is the same with centralized PD control, except the speed-dependent differential feedback gain matrix $K_d(\dot{\psi})$.

The speed-dependent differential feedback gain matrix is given by

$$K_d(\dot{\psi}) = \begin{bmatrix} k_{d1} & 0 & c_{att}I_p\dot{\psi} & 0 \\ 0 & k_{d2} & 0 & 0 \\ -c_{att}I_p\dot{\psi} & 0 & k_{d1} & 0 \\ 0 & 0 & 0 & k_{d2} \end{bmatrix} \tag{3.35}$$

where c_{att} is the attenuation ratio, which decides how much gyroscopic effects are attenuated. The closed loop system becomes

$$\begin{bmatrix} I_T & 0 & 0 & 0 \\ 0 & m & 0 & 0 \\ 0 & 0 & I_T & 0 \\ 0 & 0 & 0 & m \end{bmatrix} \ddot{q} + \begin{bmatrix} k_{d1} & 0 & (c_{att}-1)I_p\dot{\psi} & 0 \\ 0 & k_{d2} & 0 & 0 \\ (1-c_{att})I_p\dot{\psi} & 0 & k_{d1} & 0 \\ 0 & 0 & 0 & k_{d2} \end{bmatrix} \dot{q} + \begin{bmatrix} 2k_sL_B^2+k_{p1} & 0 & 0 & 0 \\ 0 & 2k_s+k_{p2} & 0 & 0 \\ 0 & 0 & 2k_sL_B^2+k_{p1} & 0 \\ 0 & 0 & 0 & 2k_s+k_{p2} \end{bmatrix} q = 0 \tag{3.36}$$

When $c_{att} = 0$, no gyroscopic effects are attenuated, the closed loop system is the same with using centralized PD controller; when $c_{att} = 1$, the gyroscopic effects are 100 % attenuated. In state variable description, the closed loop system is written as

$$\begin{bmatrix} \dot{q} \\ \ddot{q} \end{bmatrix} = \begin{bmatrix} 0 & 0 & 0 & 0 & 1 & 0 & 0 & 0 \\ 0 & 0 & 0 & 0 & 0 & 1 & 0 & 0 \\ 0 & 0 & 0 & 0 & 0 & 0 & 1 & 0 \\ 0 & 0 & 0 & 0 & 0 & 0 & 0 & 1 \\ -\frac{2k_sL_B^2+k_{p1}}{I_T} & 0 & 0 & 0 & -\frac{k_{d1}}{I_T} & 0 & (c_{att}-1)P\dot{\psi} & 0 \\ 0 & -\frac{2k_s+k_{p2}}{m} & 0 & 0 & 0 & -\frac{k_{d2}}{m} & 0 & 0 \\ 0 & 0 & -\frac{2k_sL_B^2+k_{p3}}{I_T} & 0 & (1-c_{att})P\dot{\psi} & 0 & -\frac{k_{d3}}{I_T} & 0 \\ 0 & 0 & 0 & -\frac{2k_s+k_{p4}}{m} & 0 & 0 & 0 & -\frac{k_{d4}}{m} \end{bmatrix} \begin{bmatrix} q \\ \dot{q} \end{bmatrix} \tag{3.37}$$

When the gyroscopic effects are 100 % attenuated, the closed loop system becomes linear time invariant.

3.4 Simulations results

The model data is given by Table B.1. The value of factor p is 0.5.

3.4.1 Local PD controller v.s. centralized PD controller

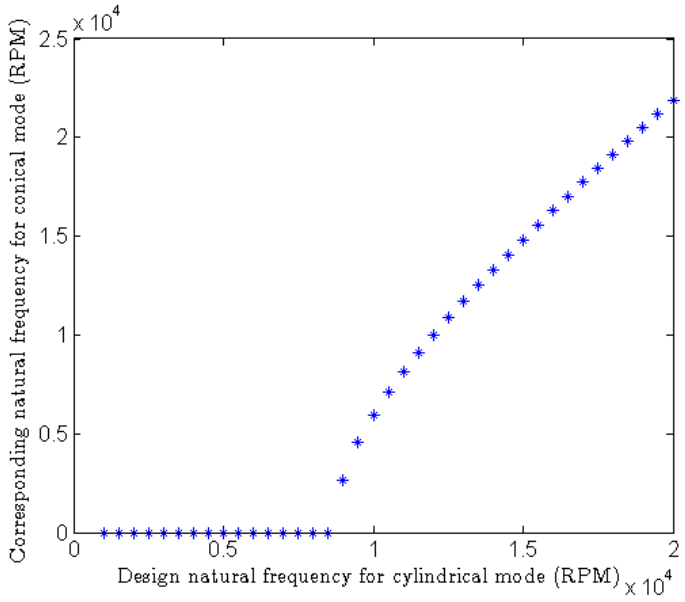

Figure 3.14: ω_n^{con} v.s. ω_n^{cyl} for local PD control

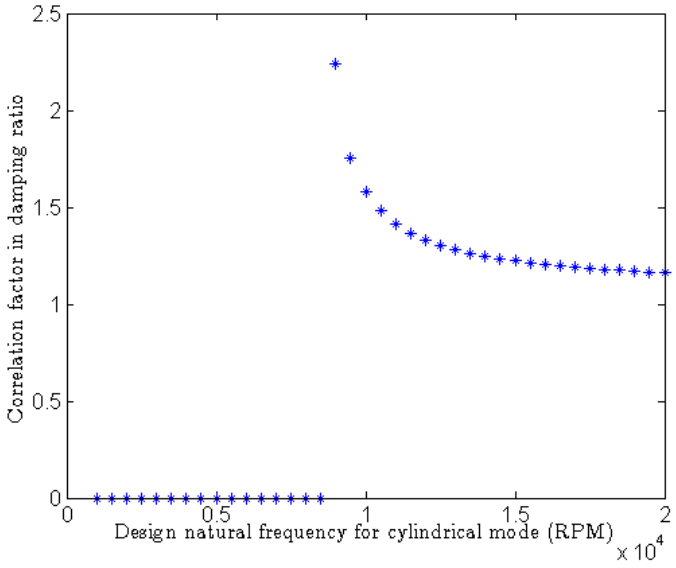

Figure 3.15: $\frac{\zeta^{con}}{\zeta^{cyl}}$ v.s. ω_n^{cyl} for local PD control

symbol	value	unit
ζ^{cyl}	0.4	N/A
ω_n^{cyl}	8800	RPM

Table 3.3: Design parameters for local PD controller

symbol	value	unit
ζ^{con}	0.5	N/A
ζ^{cyl}	0.4	N/A
ω_n^{cyl}	1200	RPM
ω_n^{con}	3500	RPM

Table 3.4: Design parameters for centralized PD controller

When applying local PD control, the relationships between system parameters in cylindrical mode and conical mode are shown in Fig.3.14 and Fig.3.15. The zero points in the figures represent that those choices of design natural frequency for cylindrical mode lead to instability in conical mode. To avoid instability and overdamping in conical mode, the natural frequency for cylindrical mode need to be larger than 8200 RPM, while the damping ratio for cylindrical mode need to be smaller than 0.5, which are very 'unbalanced'. Let the design parameters for local PD controller be given by Table 3.3, and the design parameters for centralized PD controller be given by Table 3.4.

In simulation, the rotor with 0.02 % unbalance accelerates from 0 RPM to 7500 RPM in 15 seconds. Fourth order Runge-Kutta method with fixed step size of 0.0002 is used for solving the continuous dynamic system. The following simulation results are obtained

According to Fig.3.16, the amplitude of displacement using local PD controller is smaller than the one using centralized PD controller. This is because the design natural frequency in local PD controller need to be very large in order to avoid instability, which results in a low amplitude of displacement. According to Fig.3.17, the response in conical mode using local PD is slower than the one using centralized PD. This is because the restriction in $\frac{\zeta^{con}}{\zeta^{cyl}}$ using local PD controller results in a high value of ζ^{con}. From Fig.3.18, at the 0 second, local PD controller need 42 % control-to-bias ratio to stabilize the rotor, while centralized

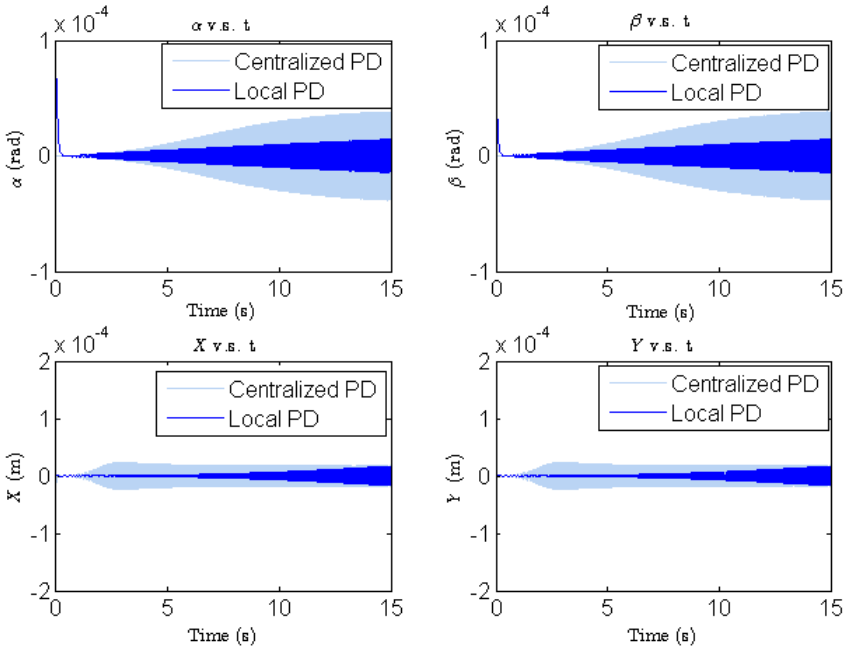

Figure 3.16: Comparison of displacement using local PD control and centralized PD control

PD controller need only 25 %. The control-to-bias ratio of local PD controller from the 1st second to the 12nd second is smaller than the one of centralized PD controller, because of the lower amplitude in displacement. However, with the increase of unbalance excitation amplitude, the control-to-bias ratio of local PD controller increases very fast, and becomes greater than the one of centralized PD at the 12nd second. Collectively, centralized PD controller leads to a better system performance.

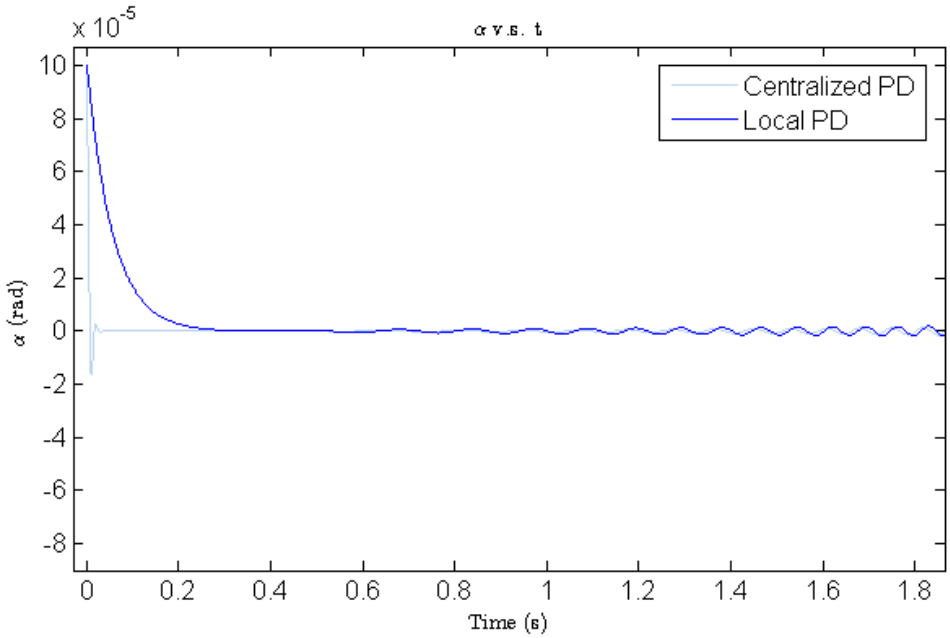

Figure 3.17: Slow response in α using local PD control

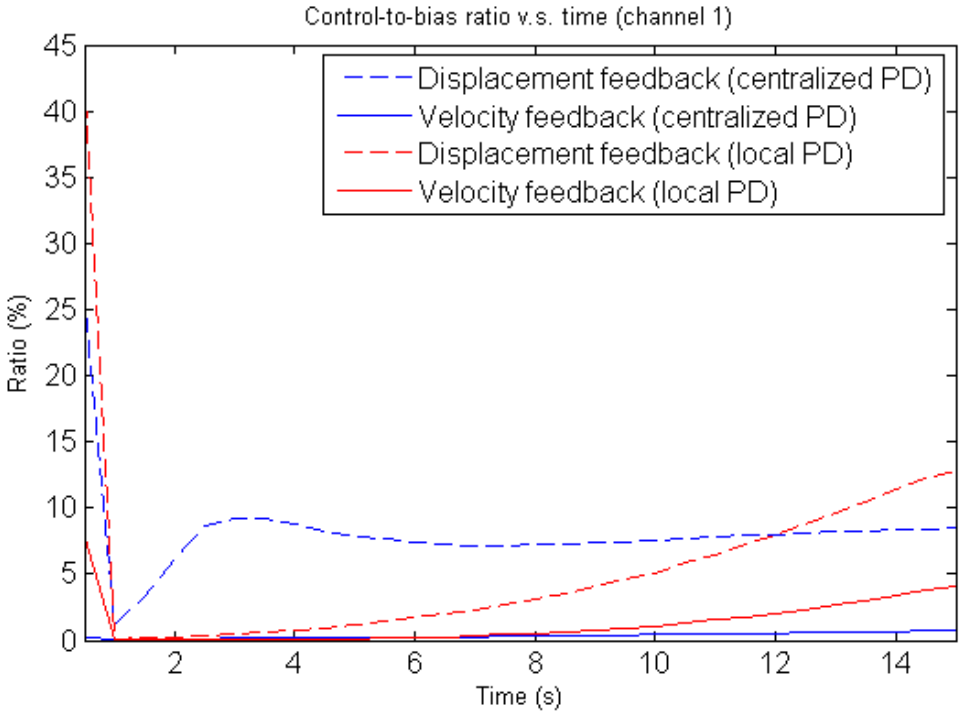

Figure 3.18: Comparison of control-to-bias ratio using local PD control and centralized PD control

3.4.2 Active gyroscopic effect attenuation

Unbalance response

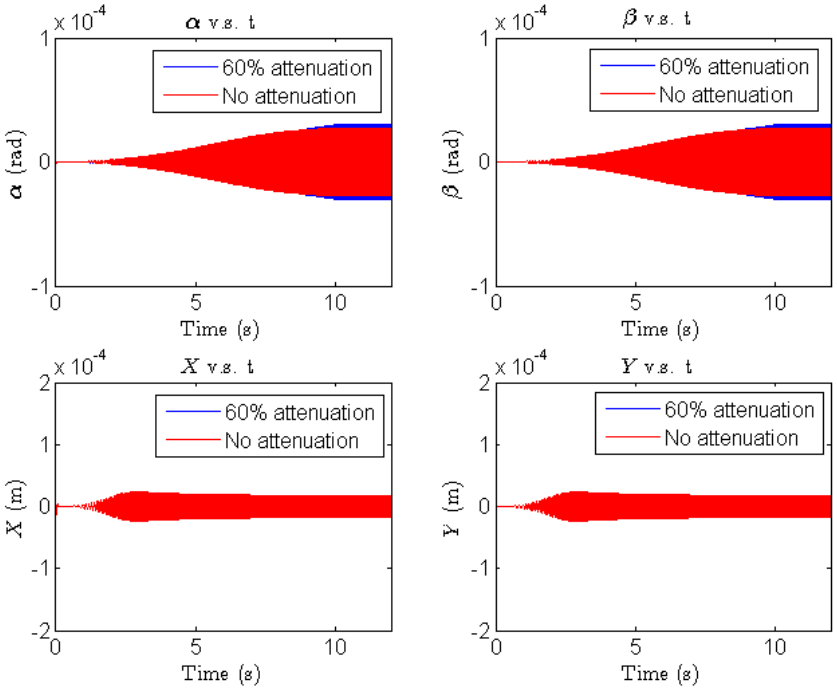

Figure 3.19: Comparison of the unbalance response with and without gyroscopic effects attenuation

In this simulation, the rotor with 0.02 % unbalance accelerates from 0 RPM to 5000 RPM in 10 seconds, then it stays at 5000 RPM for 2 seconds. The factor p is attenuated from 0.5 to 0.2 using the speed-dependent feedback gain matrix. In Fig.3.19, compared to no attenuation, the amplitude of displacement in conical mode is slightly reduced when the attenuation is activated. In Fig.3.20, the improvement in amplitude only costs 1 % more in control-to-bias ratio.

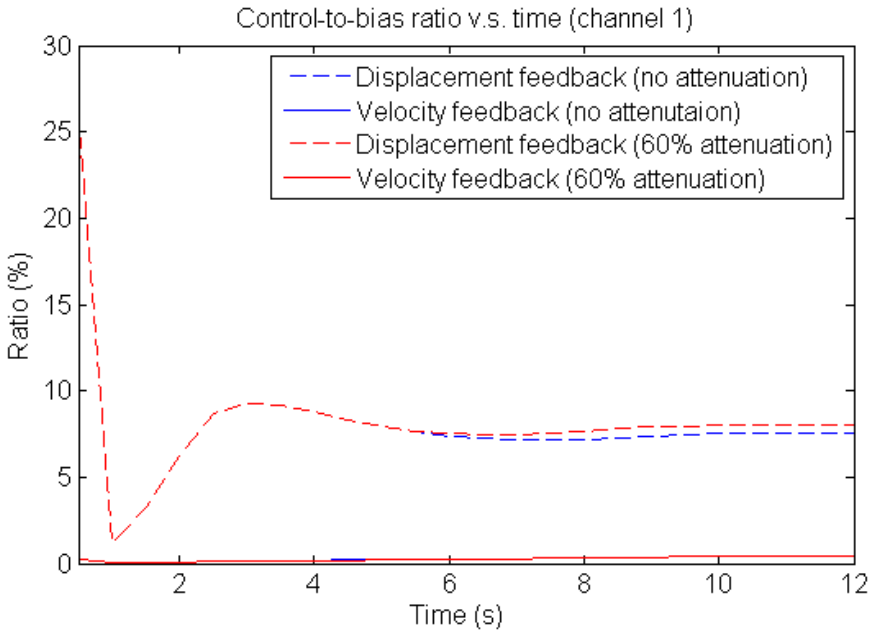

Figure 3.20: Comparison of the control-to-bias ratio with and without gyroscopic effects attenuation

Static load response

Static force with amplitude of 5 N, and static torque with amplitude of 0.75 N·m are acted periodically on the translational variable X and the rotational variable α.

In Fig.3.21, when there is attenuation, the coupling effect in two variables of conical mode reduces. Therefore, less impulse disturbance is introduced to β. Fig.3.22 shows that the improvement cost almost no control current.

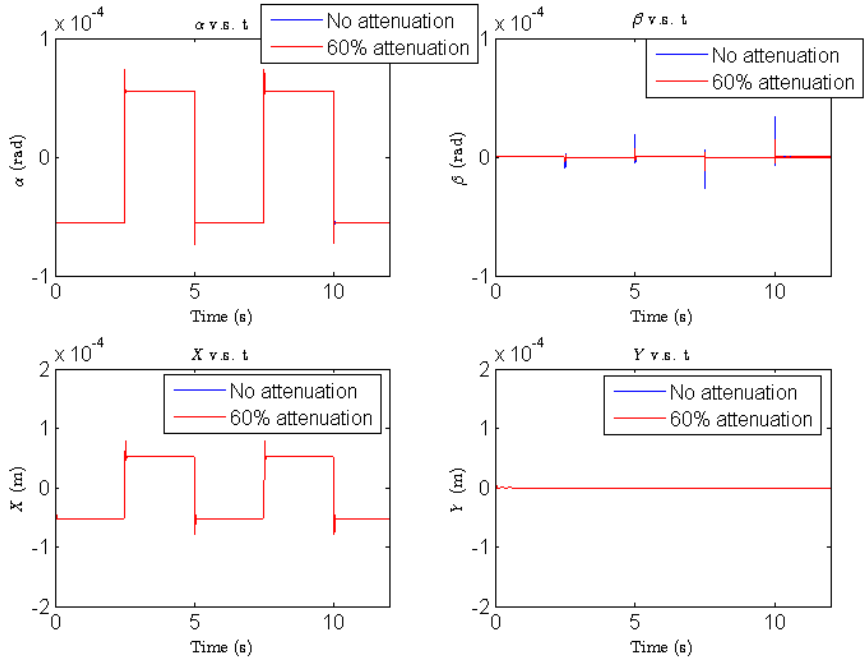

Figure 3.21: Comparison of the static load response with and without gyroscopic attenuation in the controller

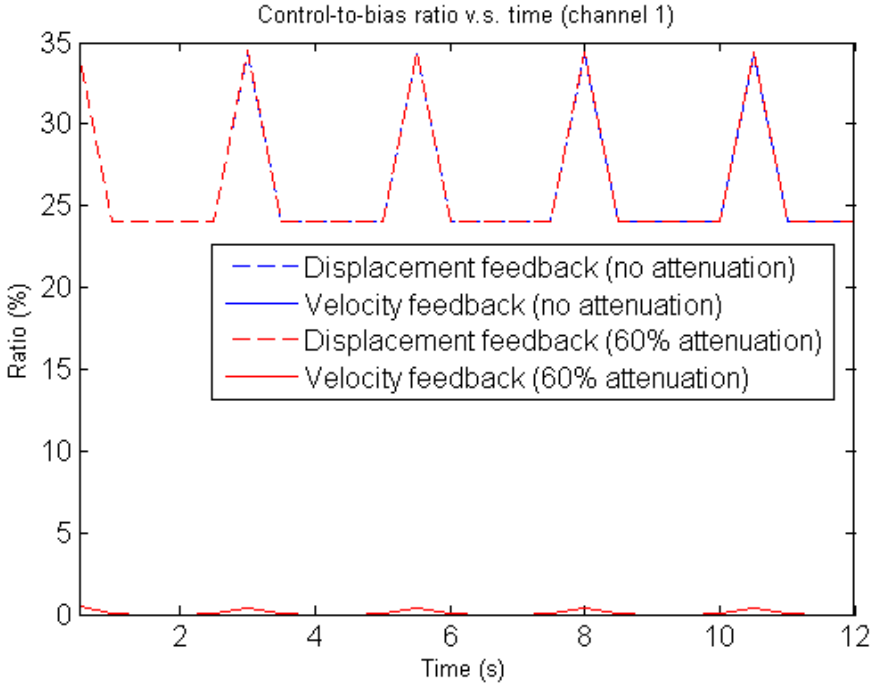

Figure 3.22: Comparison of the control-to-bias ratio with and without gyroscopic attenuation in the controller

3.5 The necessity for unbalance disturbance rejection

Once the unbalance of rotor becomes too large, stabilizing control alone will fail the system by consuming too much control current. In this simulation, the unbalance ratio is increased from 0.02 % to 0.2 %. The rotor accelerates from 0 RPM to 5000 RPM in 10 seconds, then it stays at 5000 RPM for 2 seconds. The following simulation results are obtained.

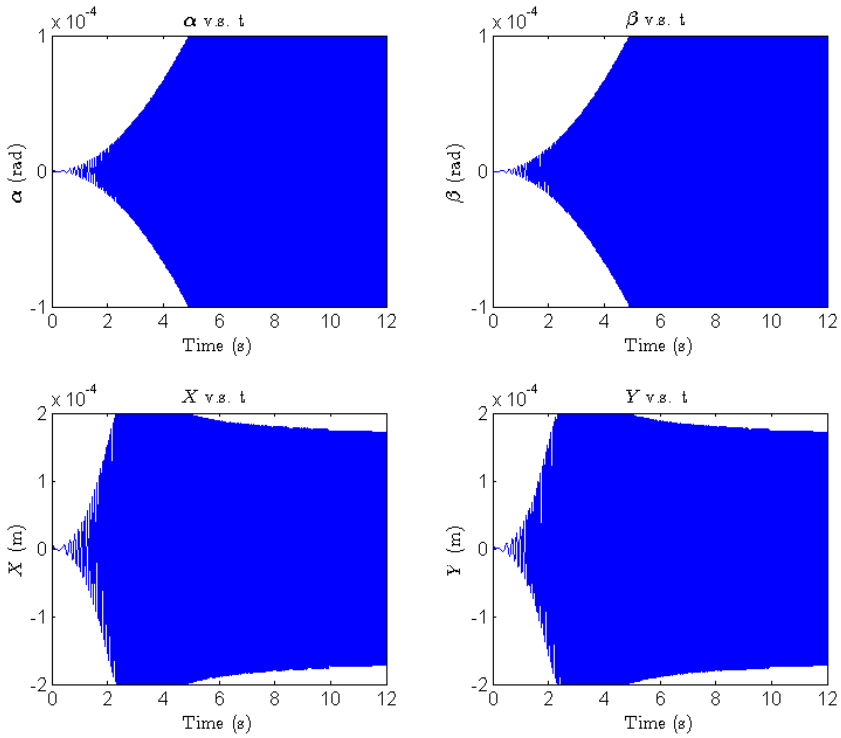

Figure 3.23: Unbalance response when unbalance ratio is large

Fig.3.23 shows a large amplitude of displacement in both two modes. In reality, the rotor will touch down on the AMBs and break the machine. Fig.3.24 shows a large control-to-bias ratio, which is even larger than 90 % in the 3rd second. In reality, the actuator will saturate very fast. Therefore, stabilizing control alone can not deal with the situation where unbalance is large. An unbalance disturbance rejection controller is desired to be added.

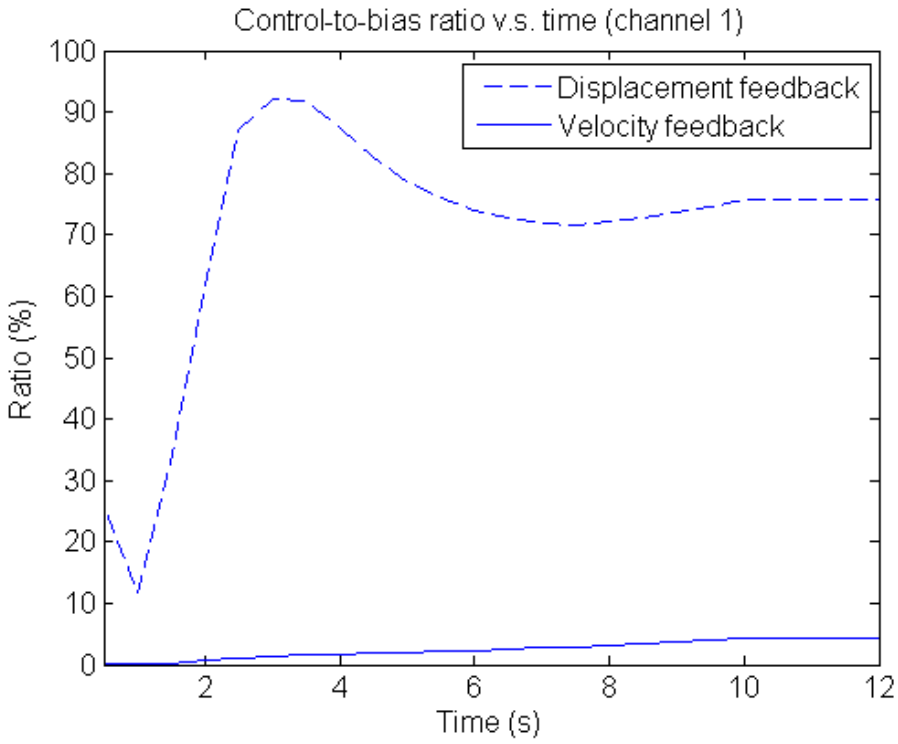

Figure 3.24: Control-to-bias ratio when unbalance ratio is large

Chapter 4

Adaptive disturbance rejection design

In the previous chapter, a stabilizing controller is designed for transient AMB system. In this chapter, an adaptive disturbance rejection controller will be designed to construct an adaptive system along with the stabilizing controller. Although there is nothing related to 'adaptive' in the stabilizing controller, it actually effects the performance of the overall adaptive system.

In the first part of this chapter, an adaptive controller, which falls in the category of model reference adaptive system (MRAS), is designed using Lyapunov theory to reject sinusoidal disturbances with time-varying frequency and time-varying magnitude. In the second part of this chapter, the adaptive controller will be implemented on an AMB system with acceleration period. Simulation results are then provided to show the performances of the adaptive system.

4.1 A MRAS design for rejecting sinusoidal disturbances of time-varying frequency and time-varying magnitude

4.1.1 Problem formulation

If a system is under transient disturbances, then the system is likely to be time-varying. A linear time-varying system under sinusoidal disturbances can be described by

$$\dot{x} = A(t)x + Bu + B_d u_d \tag{4.1}$$

$$y = Cx \tag{4.2}$$

where $u_d \subseteq \mathbb{R}^{p\times 1}$ is a disturbance vector consists of sinusoidal functions of time-varying frequency and amplitude; $u \subseteq \mathbb{R}^{l\times 1}$ is a control input vector; $x \subseteq \mathbb{R}^{n\times 1}$ is a state vector; $y \subseteq \mathbb{R}^{m\times 1}$ is a output vector; $A(t) \subseteq \mathbb{R}^{n\times n}$ is a state matrix; $B \subseteq \mathbb{R}^{n\times l}$ is a control input matrix; $C \subseteq \mathbb{R}^{m\times n}$ is a output matrix; $B_d \subseteq \mathbb{R}^{n\times p}$ is an unknown disturbance input matrix. Assume the following conditions are true

1. A positive definite matrix P, such that

$$A(t)^\top P + PA(t) \tag{4.3}$$

   is negative definite for all $t \in \mathbb{R}$ exists.

2. A linear transformation T such that

$$B_d = BT \tag{4.4}$$

   exists.

3. u_d can be written as

$$u_d = -E\phi_d \tag{4.5}$$

   where ϕ_d is a known regressor vector, and E is a linear transformation.

4.1.2 Design using Lyapunov theory

Define a linear control law

$$u_{adr} = K_{adr}\phi_d \tag{4.6}$$

Let $e = x - 0$ be the state error. The error system with this linear control is given by

$$\begin{aligned}\dot{e} = \dot{x} &= Ax + Bu_{adr} - B\underbrace{TE}_{K^*_{adr}}\phi_d \\ &= Ae + BK_{adr}\phi_d - BK^*_{adr}\phi_d \\ &= Ae + B\underbrace{(K_{adr} - K^*_{adr})}_{\text{The mismatch}}\phi_d\end{aligned} \tag{4.7}$$

where K^*_{adr} is the *nominal value matrix* of the adaptive gain matrix K_{adr}. Define $\Delta K = K_{adr} - K^*_{adr}$.

Using the P in Assumption 1, a positive definite function of e and ΔK is defined as

$$V = \frac{1}{2}\left(e^\top Pe + \text{tr}\left[\Delta K \Delta K^\top\right]\right) \tag{4.8}$$

Taking first derivative of V with respect to time, yields

$$\begin{aligned}\dot{V} &= \frac{1}{2}\left(\dot{e}^\top Pe + \text{tr}[\Delta\dot{K}\Delta K^\top]\right) \\ &= \frac{1}{2}e^\top\left[A(t)^\top P + PA(t)\right]e + \phi_d^\top \Delta K^\top B^\top Pe + \text{tr}[\Delta\dot{K}\Delta K^\top]\end{aligned}$$

Using the fact that

$$x^\top y = \text{tr}[yx^\top] \tag{4.9}$$

where x and y are two vectors of same dimension. We have

$$\dot{V} = \frac{1}{2}e^\top\left[A(t)^\top P + PA(t)\right]e + \text{tr}[(B^\top Pe\phi_d^\top + \Delta\dot{K})\Delta K^\top] \tag{4.10}$$

4.1.3 The control law using output feedback

If

$$B^\top P = C \tag{4.11}$$

is true for the model, Eq. 4.10 can be written as

$$\dot{V} = \frac{1}{2}e^\top \left[A(t)^\top P + PA(t)\right] e + \text{tr}[(e_y\phi_d^\top + \Delta\dot{K})\Delta K^\top] \tag{4.12}$$

where $e_y = Ce$ is the output error.

Letting

$$\Delta\dot{K} = -e_y\phi_d^\top \tag{4.13}$$

$\dot{V}$ becomes

$$\dot{V} = \frac{1}{2}e^\top \left[A(t)^\top P + PA(t)\right] e \tag{4.14}$$

which is negative semidefinite. By *Lyapunov theory*, e and ΔK are bounded.

Taking second derivative of V with respect to time, yields

$$\begin{aligned}\ddot{V} =& \frac{1}{2}e^\top \left\{A(t)^\top [A(t)^\top P + PA(t)]\right\} e \\ &+ \frac{1}{2}e^\top \left\{[A(t)^\top P + PA(t)]A(t)\right\} e \\ &+ \frac{1}{2}e^\top [\dot{A}^\top(t)P + P\dot{A}(t)]e \\ &+ \phi_d^\top \Delta K^\top \bar{B}^\top [A(t)^\top P + PA(t)]e\end{aligned} \tag{4.15}$$

We already have the following

- e and ΔK are bounded.

Therefore, if the regressor ϕ_d and $||\dot{A}(t)||$ is bounded, $\ddot{V}$ will be bounded. Therefore, by *Barbalat's lemma*, $\dot{V} \to 0$ as $t \to \infty$, which means $e \to 0$ as $t \to \infty$.

In summary, the adaptive control law using *output feedback* and *feedforward regressor vector* is given by

$$u_{adr} = K_{adr}\phi_d \tag{4.16}$$

along with the adaptive gain law

$$\Delta\dot{K}_{adr} = -e_y\phi_d^\top \tag{4.17}$$

4.1.4 The control law using state feedback

When the condition in Eq. 4.11 is not true, output feedback is not available, then state feedback has to be used. Letting

$$\Delta\dot{K} = -B^\top P e \phi_d^\top \tag{4.18}$$

$\dot{V}$ becomes

$$\dot{V} = -\frac{1}{2} e^\top Q e \tag{4.19}$$

which is negative semidefinite. By *Lyapunov theory*, e and ΔK are bounded.
Taking second derivative of V with respect to time, yields

$$\begin{aligned}
\ddot{V} =& \frac{1}{2} e^\top \left\{ A(t)^\top [A(t)^\top P + P A(t)] \right\} e \\
&+ \frac{1}{2} e^\top \left\{ [A(t)^\top P + P A(t)] A(t) \right\} e \\
&+ \frac{1}{2} e^\top [\dot{A}^\top(t) P + P \dot{A}(t)] e \\
&+ \phi_d^\top \Delta K^\top \bar{B}^\top [A(t)^\top P + P A(t)] e
\end{aligned} \tag{4.20}$$

We already have the following

- e and ΔK are bounded.

Therefore, if the regressor ϕ_d and $||\dot{A}(t)||$ is bounded. Then by *Barbalat's lemma*, $\dot{V} \to 0$ as $t \to \infty$, which means $e \to 0$ as $t \to \infty$.
In summary, the adaptive control law using *state feedback* and *feedforward regressor vector* is given by

$$u_{adr} = K_{adr} \phi_d \tag{4.21}$$

along with the adaptive gain law

$$\dot{K}_{adr} = -B^\top P e \phi_d^\top \tag{4.22}$$

4.2 Application of the MRAS design to a stabilized AMB system

4.2.1 Formulation

Adaptive disturbance rejection is desired to be superposed into the stabilized AMB system to reject unbalance disturbances during acceleration.

The closed loop AMB system stabilized by centralized PD control can be written as

$$M\ddot{q} + (G(\dot{\psi}) + K_d)\dot{q} + (BK_sB^\top + K_p)q = BK_ii + B_du_d \tag{4.23}$$

Let the adaptive control current be

$$i_{adr} = T_{out}Mu_{adr} \tag{4.24}$$

where

$$T_{out} = (BK_i)^{-1} \tag{4.25}$$

The state variable description of the closed loop system is transformed into

$$\underbrace{\begin{bmatrix}\dot{q}\\ \ddot{q}\end{bmatrix}}_{\dot{x}} = \underbrace{\begin{bmatrix}\varnothing & I\\ M^{-1}(BK_sB^\top + K_p) & M^{-1}(G(\dot{\psi}) + K_d)\end{bmatrix}}_{A_{cl,ss}(\dot{\psi})}\underbrace{\begin{bmatrix}q\\ \dot{q}\end{bmatrix}}_{x} + \underbrace{\begin{bmatrix}\varnothing\\ I\end{bmatrix}}_{\bar{B}_{ss}}u_{adr} + \underbrace{\begin{bmatrix}\varnothing\\ M^{-1}B_d\end{bmatrix}}_{B_{d,ss}}u_d \tag{4.26}$$

$$y = \underbrace{\begin{bmatrix}C & \varnothing\end{bmatrix}}_{C_{ss}}x \tag{4.27}$$

where

$$A_{cl,ss}(\dot{\psi}) = \begin{bmatrix} 0 & 0 & 0 & 0 & 1 & 0 & 0 & 0 \\ 0 & 0 & 0 & 0 & 0 & 1 & 0 & 0 \\ 0 & 0 & 0 & 0 & 0 & 0 & 1 & 0 \\ 0 & 0 & 0 & 0 & 0 & 0 & 0 & 1 \\ -\frac{2k_sL_B^2+k_{p1}}{I_T} & 0 & 0 & 0 & -\frac{k_{d1}}{I_T} & 0 & \frac{I_P}{I_T}\dot{\psi} & 0 \\ 0 & -\frac{2k_s+k_{p2}}{m} & 0 & 0 & 0 & -\frac{k_{d2}}{m} & 0 & 0 \\ 0 & 0 & -\frac{2k_sL_B^2+k_{p1}}{I_T} & 0 & -\frac{I_P}{I_T}\dot{\psi} & 0 & -\frac{k_{d1}}{I_T} & 0 \\ 0 & 0 & 0 & -\frac{2k_s+k_{p2}}{m} & 0 & 0 & 0 & -\frac{k_{d2}}{m} \end{bmatrix}$$

$$\bar{B}_{ss} = \begin{bmatrix} 0 & 0 & 0 & 0 \\ 0 & 0 & 0 & 0 \\ 0 & 0 & 0 & 0 \\ 0 & 0 & 0 & 0 \\ 1 & 0 & 0 & 0 \\ 0 & 1 & 0 & 0 \\ 0 & 0 & 1 & 0 \\ 0 & 0 & 0 & 1 \end{bmatrix}$$

$$B_{d,ss} = \begin{bmatrix} 0 & 0 \\ 0 & 0 \\ 0 & 0 \\ 0 & 0 \\ \frac{m_u u_x u_z}{I_T} & \frac{m_u u_y u_z}{I_T} \\ \frac{m_u u_x}{m} & \frac{m_u u_y}{m} \\ -\frac{m_u u_y u_z}{I_T} & \frac{m_u u_x u_z}{I_T} \\ \frac{m_u u_y}{m} & -\frac{m_u u_x}{m} \end{bmatrix}$$

$$C_{ss} = \begin{bmatrix} L_S & 1 & 0 & 0 & 0 & 0 & 0 & 0 \\ -L_S & 1 & 0 & 0 & 0 & 0 & 0 & 0 \\ 0 & 0 & -L_S & 1 & 0 & 0 & 0 & 0 \\ 0 & 0 & L_S & 1 & 0 & 0 & 0 & 0 \end{bmatrix}$$

$$u_d = \begin{bmatrix} \dot{\psi}^2 \cos\psi + \ddot{\psi} \sin\psi \\ -\dot{\psi}^2 \sin\psi + \ddot{\psi} \cos\psi \end{bmatrix}$$

$$\dot{\psi} = \begin{cases} a(t - t_0), & t_0 < t < t_0 + t_a \\ a t_a, & t_0 + t_a \leq t < \infty \end{cases}$$

Assume rotor speed measurement Ω is available from the speed control loop for the AMB system. A regressor vector constructed by speed measurement is given by

$$\phi_d = \begin{bmatrix} \Omega^2 \cos(\int_0^t \Omega d\tau) + \dot{\Omega} \sin(\int_0^t \Omega d\tau) \\ -\Omega^2 \sin(\int_0^t \Omega d\tau) + \dot{\Omega} \cos(\int_0^t \Omega d\tau) \end{bmatrix} \tag{4.28}$$

4.2.2 Applicability

The following arguments are made corresponding to each assumption in Section 4.1.1:

1. It has been shown in Section 3.2.1 that, this positive definite matrix P exists when $\omega_n^{con}\zeta^{con}$ is large enough and $\dot{\psi}$ is bounded.

2. The required linear transformation T satisfying $\bar{B}_{ss}T = B_{d,ss}$ is given by

$$T = \begin{bmatrix} \frac{m_u u_x u_z}{I_T} & \frac{m_u u_y u_z}{I_T} \\ \frac{m_u u_x}{m} & \frac{m_u u_y}{m} \\ -\frac{m_u u_y u_z}{I_T} & \frac{m_u u_x u_z}{I_T} \\ \frac{m_u u_y}{m} & -\frac{m_u u_x}{m} \end{bmatrix} \tag{4.29}$$

3. Let $\psi_e = \psi - \int \Omega$ be the *phase error* between the real phase of unbalance disturbances and the calculated phase from speed sensor measurement. Then we have

$$u_d = -E\phi_d$$

where

$$E = \begin{bmatrix} -\cos\psi_e & \sin\psi_e \\ -\sin\psi_e & -\cos\psi_e \end{bmatrix} \tag{4.30}$$

Therefore, the MRAS can be applied to this stabilized AMB system. However, because the relationship $\bar{B}_{ss}^{\top} P = C_{ss}$ can't be found in this realization of AMB system, the MRAS need to use state feedback.

The displacement variables in state vector can be directly calculated from sensor output. A state estimator can be built to get the velocity variables. But the state estimate will be affected by the unbalance disturbances if they haven't been augmented into the estimation model. Therefore, numerical differentiation is used to calculate the velocity variables in state vector. Consequently, the sensor output need to be filtered in an appropriate way before carrying out the numerical differentiation.

The adaptive control law is given by

$$\begin{aligned} u_{adr} &= K_{adr}\phi_d \\ &= \begin{bmatrix} K_{1,1} & K_{1,2} \\ K_{2,1} & K_{2,2} \\ K_{3,1} & K_{3,2} \\ K_{4,1} & K_{4,2} \end{bmatrix} \begin{bmatrix} \Omega^2 \cos(\int_0^t \Omega d\tau) + \dot{\Omega}\sin(\int_0^t \Omega d\tau) \\ -\Omega^2 \sin(\int_0^t \Omega d\tau) + \dot{\Omega}\cos(\int_0^t \Omega d\tau) \end{bmatrix} \end{aligned} \tag{4.31}$$

along with the adaptive gain law

$$\dot{K}_{adr} = -\gamma \bar{B}_{ss}^{\top} P e \phi_d^{\top} \tag{4.32}$$

where γ is used for tunning the adaptive controller. Control current can be calculated by

$$i_{adr} = T_{out} M u_{adr}$$

In the disturbance vector, the terms with amplitude related to acceleration is much smaller than the terms with amplitude related to square of speed. Thus, the adaptive rejection of these acceleration-related terms are not always necessary. Then the regressor vector can sometimes be simplified into

$$\phi_d = \begin{bmatrix} \Omega^2 \cos(\int_0^t \Omega d\tau) \\ -\Omega^2 \sin(\int_0^t \Omega d\tau) \end{bmatrix} \tag{4.33}$$

The simplified regressor vector can avoid the numerical differentiation of rotor speed measurement.

4.2.3 Summary of the design procedures

The design procedures for the overall adaptive system are summarized as following

1. Choose design parameters ω_n^{cyl}, ω_n^{con}, ζ^{cyl} and ζ^{con} for the baseline stabilizing controller.

2. Choose a positive definite matrix Q, and numerically solve P from

$$A_{cl,ss}(0)^\top P + P A_{cl,ss}(0) = -Q$$

3. Numerically test whether

$$A_{cl,ss}(\dot{\psi}) P + P A_{cl,ss}(\dot{\psi}) \leq -\gamma I$$

where

$$\dot{\psi} = \begin{cases} at, & 0 < t < t_a \\ at_a, & t_a \leq t < \infty \end{cases}$$

is true for all $t \in [0, \infty)$.

4. Construct

$$\phi_d = \begin{bmatrix} \Omega^2 \cos(\int_0^t \Omega d\tau) \\ -\Omega^2 \sin(\int_0^t \Omega d\tau) \end{bmatrix}$$

from rotor sensor measurement.

5. Apply adaptive disturbance rejection

$$\begin{aligned} u_{adr} &= K_{adr}\phi_d \\ &= \begin{bmatrix} k_{1,1} & k_{1,2} \\ k_{2,1} & k_{2,2} \\ k_{3,1} & k_{3,2} \\ k_{4,1} & k_{4,2} \end{bmatrix} \begin{bmatrix} \Omega^2 \cos(\int_0^t \Omega d\tau) \\ -\Omega^2 \sin(\int_0^t \Omega d\tau) \end{bmatrix} \end{aligned}$$

along with the adaptive gain law

$$\dot{K}_{adr} = -\gamma \bar{B}_{ss}{}^{\top} P e \phi_d^{\top}$$

where the scalar γ is used for tunning.

6. The control current is calculated by

$$i_{adr} = T_{out} M u_{adr}$$

4.3 Simulation results

In simulation, the model data is given by Table B.1. The factor p is equal to 0.5. The rotor with 0.2 % unbalance accelerates from 0 RPM to 5000 RPM in 10 seconds, then it stays at 5000 RPM for 2 seconds. Fourth order Runge-Kutta method with fixed step size of 0.0002 is used for solving the continuous dynamic system. Different controller design parameters are tested under different situations to investigate the performance of this adaptive control system.

4.3.1 Noise-free, delay-free situation

Symbol	Value	Unit
ω_n^{cyl}	1200	RPM
ω_n^{con}	3500	RPM
ζ^{cyl}	0.4	N/A
ζ^{con}	0.5	N/A
Q	eye(8,8)	N/A
γ	1e-2	N/A

Table 4.1: Parameters for control design

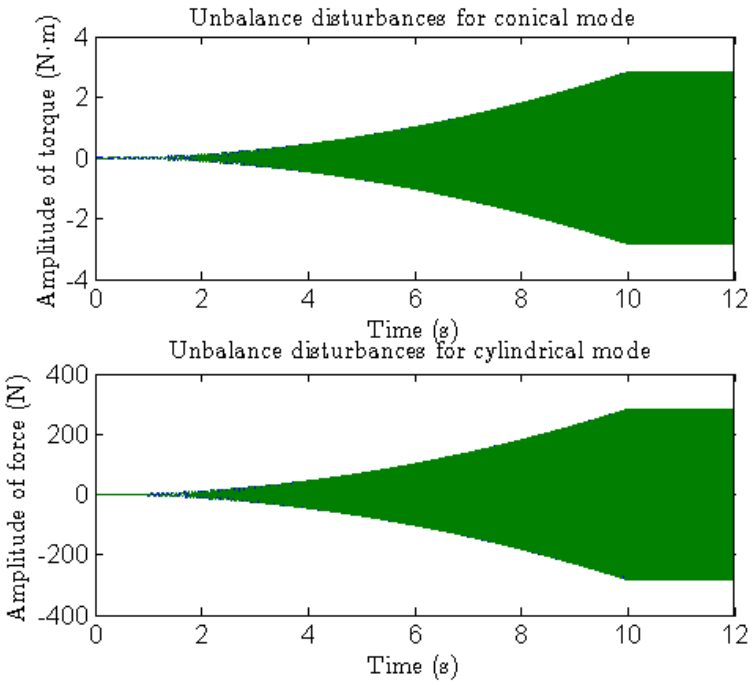

Figure 4.1: Unbalance disturbances during start-up

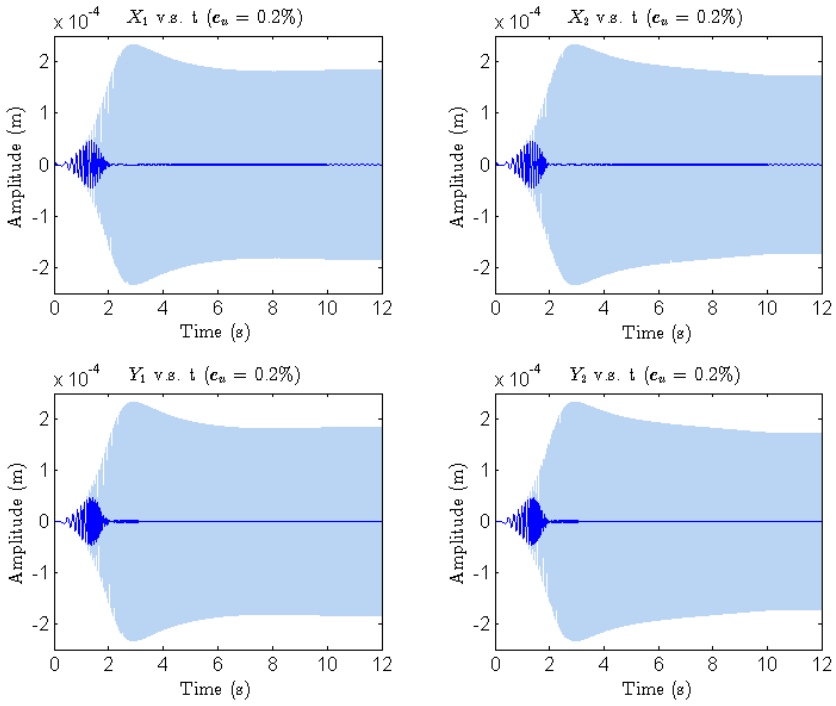

Figure 4.2: The evident improvement in amplitude of displacement when there is ADR (blue) compared to no ADR (light blue)

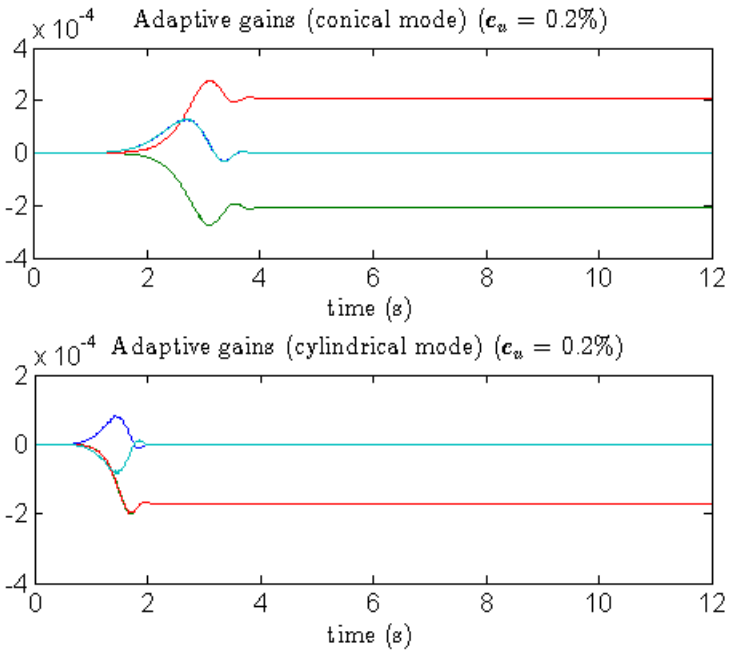

Figure 4.3: The convergence of adaptive gains

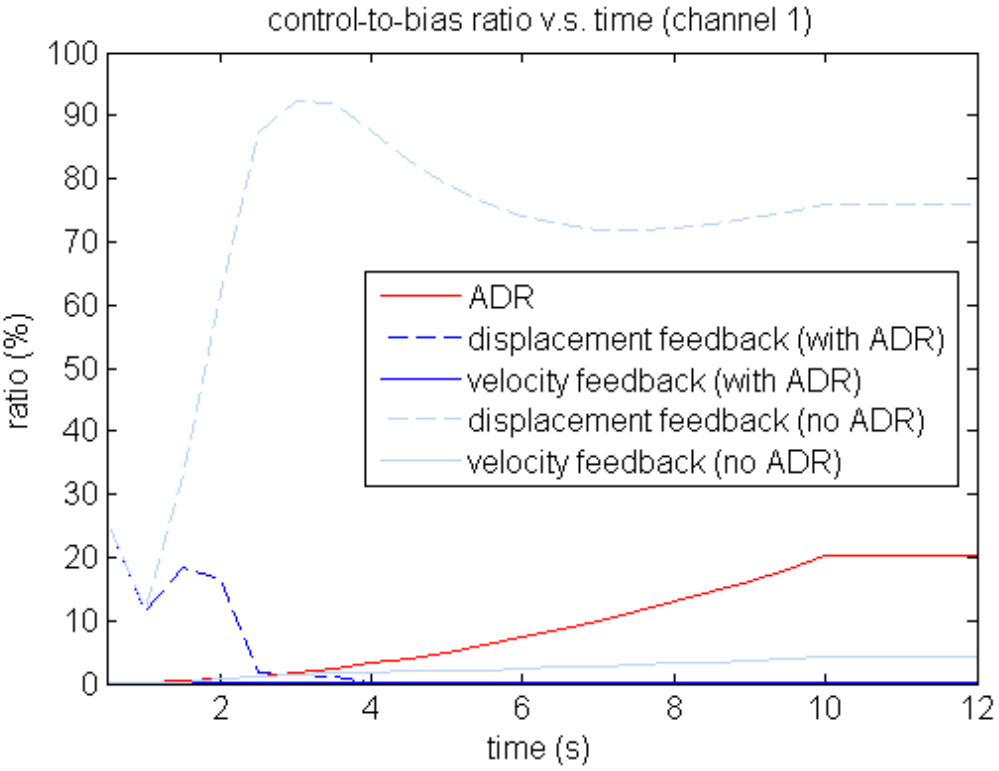

Figure 4.4: The evident improvement in current consumption

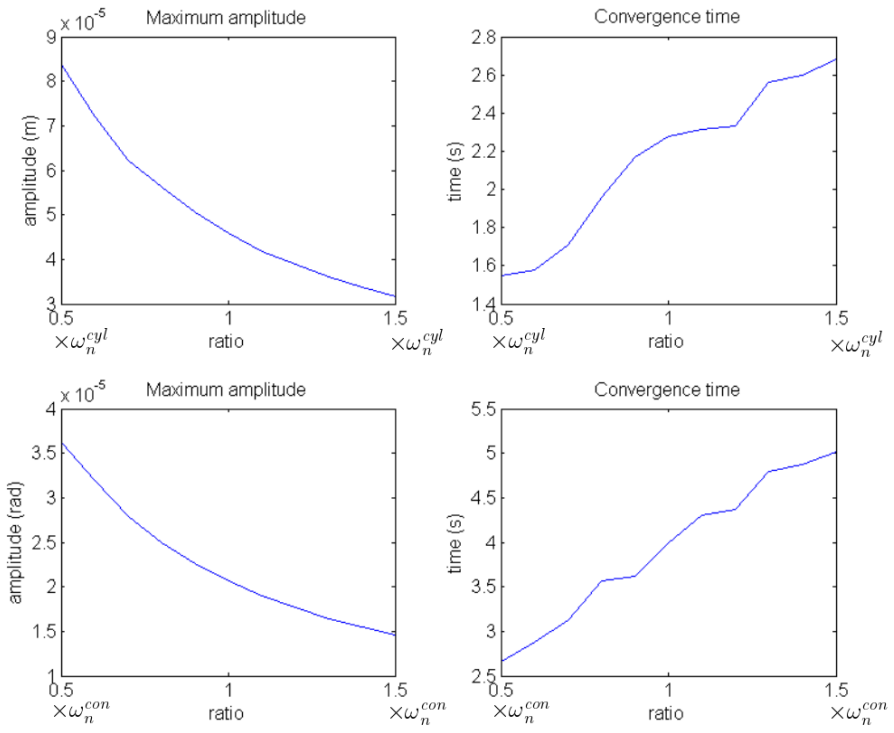

Figure 4.5: Effects of stabilizing controller parameters

Comments

The sinusoidal disturbances of time-varying frequency and amplitude during acceleration are shown in Fig.4.1. In Fig.4.2, a comparison of translational displacement in bearing planes between using ADR and using stabilizing controller alone is presented. The peak amplitude of the vibration reduces 90 % when ADR is used. Fig.4.4 shows the control current consumption decreases 80 % when ADR is used.

Fig.4.5 shows the effects of the stabilizing controller to the overall adaptive system. For both conical mode variables and cylindrical mode variables, when the designed natural frequencies are chosen to be smaller, the convergence time of adaptive gains becomes shorter, but the maximum amplitude of displacement becomes larger; when the designed natural frequencies are chosen to be larger, the convergence time of adaptive gains becomes longer, but the maximum amplitude of displacement becomes smaller. This can be explained by the 'exciting level' of the stabilized system corresponding to different sets of designed parameters. When natural frequency is chosen to be small. The state variables will be large before convergence, that is, the state variables become more 'exciting', which makes the adaptive gains easier to converge. When natural frequency is chosen to be large. The state variables will be small before convergence, that is, the state variables become more 'boring', which makes the adaptive gains harder to converge.

4.3.2 Considering process noise and sensor noise

Formulation

A process noise from electromagnets is described by

$$\text{Process noise} = B_{ss} \begin{bmatrix} w \\ w \\ w \\ w \end{bmatrix} \tag{4.34}$$

where $w \sim N(0, (0.001)^2)$.

The sensor noise in proximity sensors is described by

$$\text{Sensor noise} = \begin{bmatrix} v \\ v \\ v \\ v \end{bmatrix} \tag{4.35}$$

where $v \sim N(0, (1e-7)^2)$.

Therefore, the system can be formulated as

$$\underbrace{\begin{bmatrix} \dot{q} \\ \ddot{q} \end{bmatrix}}_{\dot{x}} = \underbrace{\begin{bmatrix} \varnothing & I \\ M^{-1}(BK_sB^\top + K_p) & M^{-1}(G(\dot{\psi}) + K_d) \end{bmatrix}}_{A_{cl,ss}(\dot{\psi})} \underbrace{\begin{bmatrix} q \\ \dot{q} \end{bmatrix}}_{x} + \underbrace{\begin{bmatrix} \varnothing \\ I \end{bmatrix}}_{\bar{B}_{ss}} u_{adr} + \underbrace{\begin{bmatrix} \varnothing \\ M^{-1}B_d \end{bmatrix}}_{B_{d,ss}} u_d + B_{ss}w \tag{4.36}$$

$$y = \underbrace{\begin{bmatrix} C & \varnothing \end{bmatrix}}_{C_{ss}} x + v \tag{4.37}$$

Results

Simulation results are given by

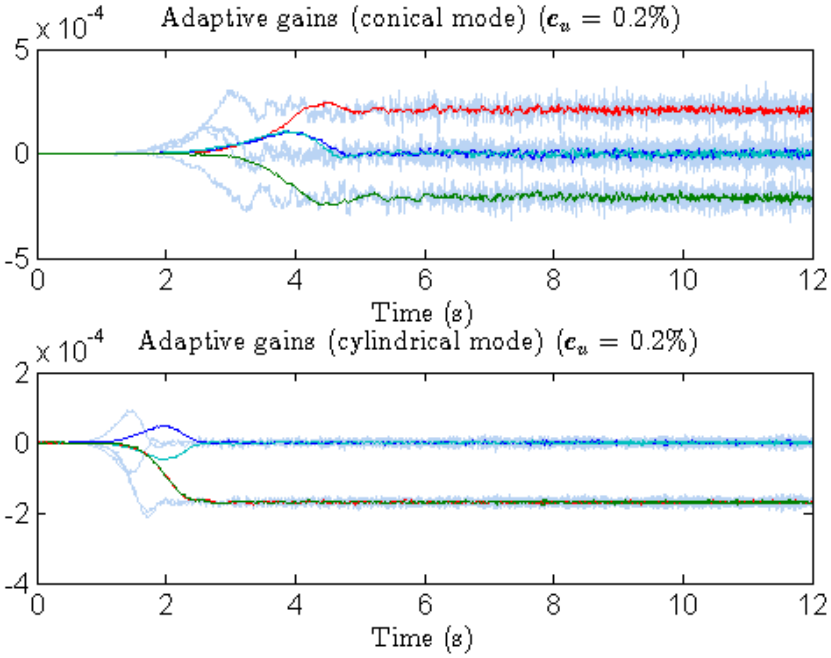

Figure 4.6: The larger $\gamma = 1e-2$ (light color) results in a faster convergence but noisier adaptive gains compared to the smaller $\gamma = 1e-3$ (dark color)

Comments

Firstly, the adaptive control system is robust under sufficiently small process noise and sensor noise. Secondly, a smaller tunning gain γ can reduce the amount of noise going into the adaptive gains and translational variables. However, a smaller tunning gain also makes the convergence of adaptive gains slower, which results in a larger vibration peak.

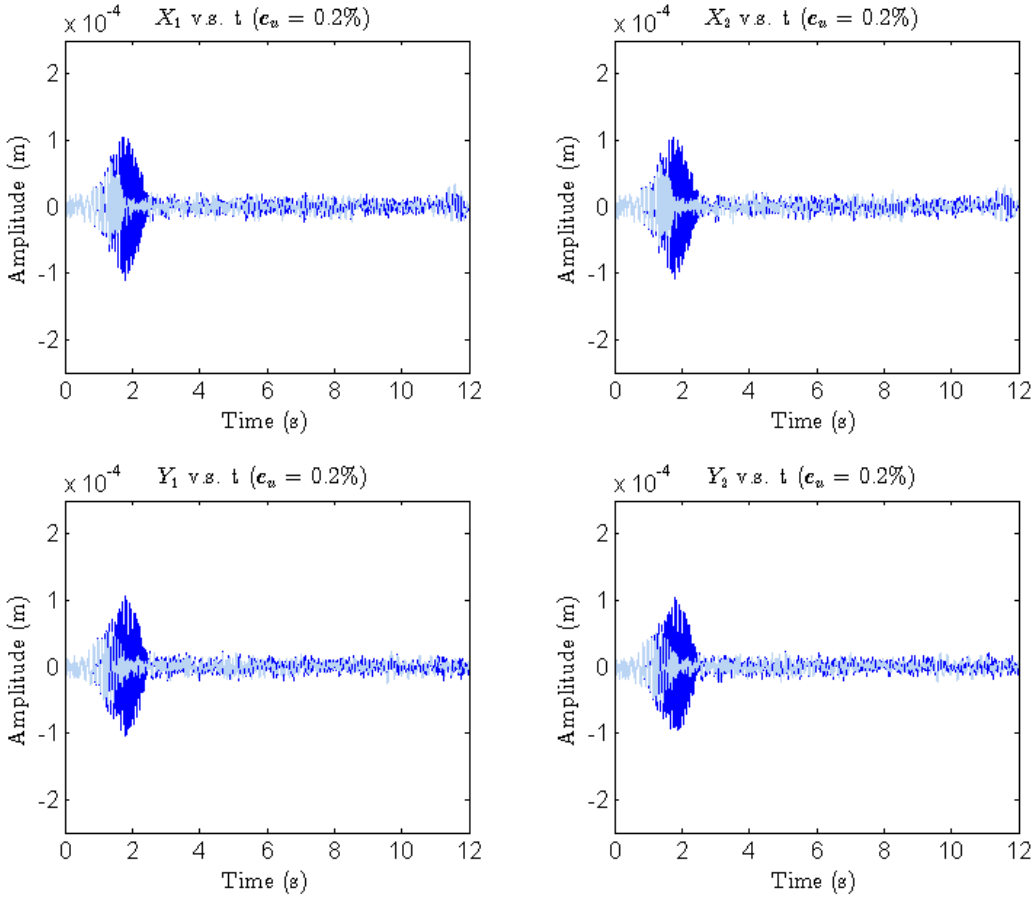

Figure 4.7: The larger $\gamma = 1e-2$ (light color) results in a lower maximum amplitude but a higher amplitude in general compared to the smaller $\gamma = 1e-3$ (dark color)

4.3.3 Considering delay in rotor speed measurement

Let the delay in speed sensor measurement be 0.1 second. The parameters for control design are adjusted as Table 4.2.

Symbol	Value	Unit
ω_n^{cyl}	1200	RPM
ω_n^{con}	3500	RPM
ζ^{cyl}	0.4	N/A
ζ^{con}	0.5	N/A
Q	eye(8,8)	N/A
γ	1e-4	N/A

Table 4.2: Parameters for control design

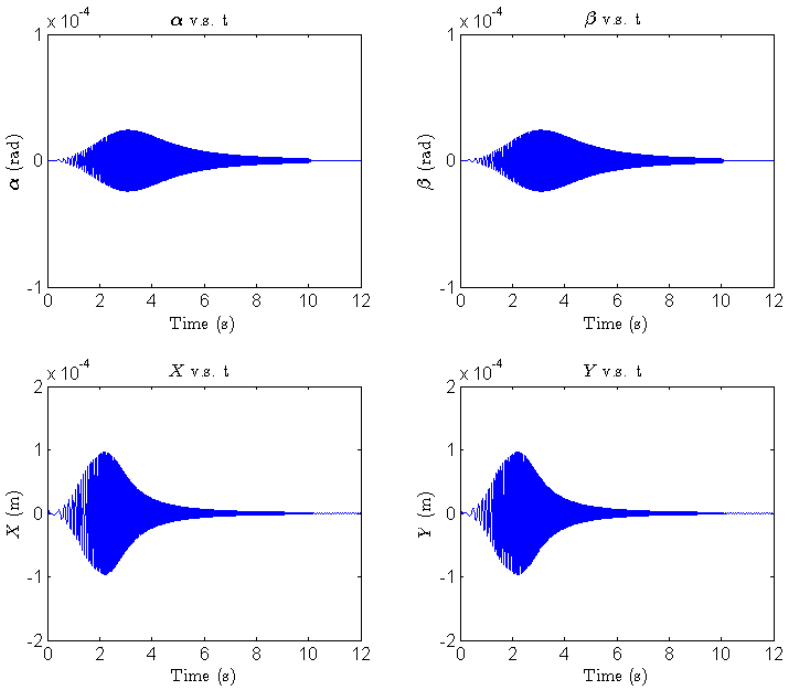

Figure 4.8: Amplitude of the displacement is decreasing even though there is delay in speed measurement

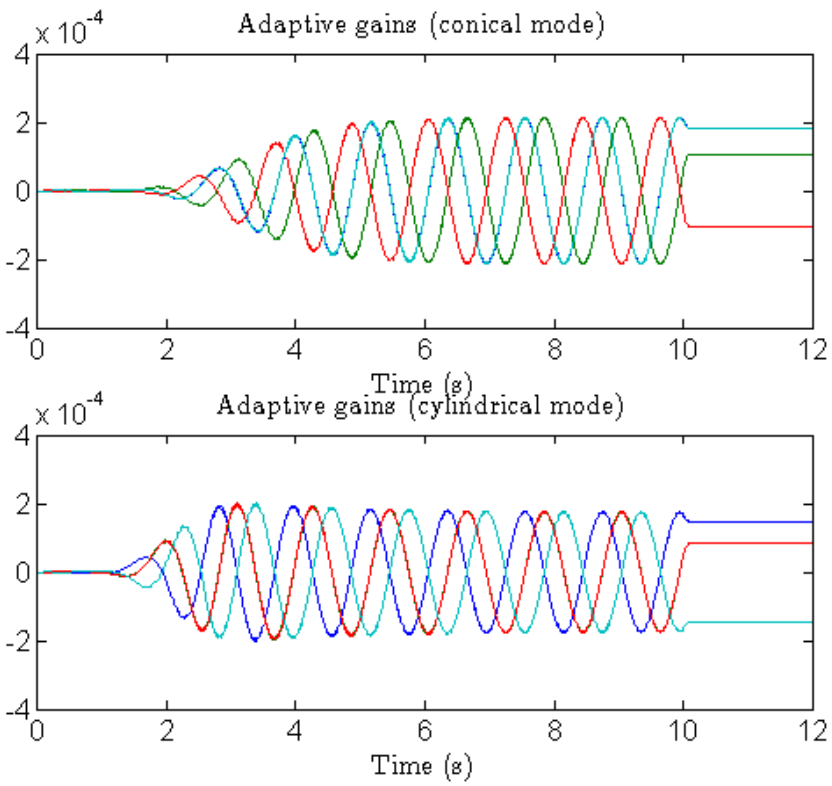

Figure 4.9: The adaptive gains are tracking some sinusoidal functions during transient period

Explanation of the 'sinusoidal tracking' behavior in adaptive gains

From the simulation results, when there is delay in speed measurement, the adaptive controller still has effect in rejecting the disturbances. The adaptive gains converge to some sinusoidal functions. When the delay is longer, it takes longer time to converge. This 'sinusoidal tracking' behavior in adaptive gains can be explained analytically.

Recall that, when there is no delay in rotor speed measurement, the disturbance vector u_d and the regressor vector ϕ_d have the following relationship

$$u_d = -E\phi_d \tag{4.38}$$

where E is the matrix compensates the phase error between the disturbance vector and the regressor vector.

The nominal value of adaptive gain matrix can be written as

$$K^*_{adr} = TE \tag{4.39}$$

When there is delay in rotor speed measurement, the delayed disturbance vector u_{dd} has the following relationship with the delayed regressor vector phi_{dd}

$$u_{dd} = -E\phi_{dd} \tag{4.40}$$

The delayed disturbance vector is given by

$$\begin{aligned} u_{dd} &= \begin{bmatrix} \dot{\psi}^2(t-\Delta t)\cos(\int_{t_0}^{t-\Delta t}\dot{\psi}dt) \\ -\dot{\psi}^2(t-\Delta t)\sin(\int_{t_0}^{t-\Delta t}\dot{\psi}dt) \end{bmatrix} \\ &= (\dot{\psi} - \underbrace{\int_{t_0}^{t-\Delta t}\ddot{\psi}dt}_{\delta})^2 \begin{bmatrix} \cos(\psi - \int_{t-\Delta t}^{t}\dot{\psi}dt) \\ -\sin(\psi - \int_{t-\Delta t}^{t}\dot{\psi}dt) \end{bmatrix} \end{aligned} \tag{4.41}$$

Assuming Δt is small, then δ is small, u_{dd} can be written as

$$u_{dd} \approx \underbrace{\begin{bmatrix} \cos(\int_{t-\Delta t}^{t}\dot{\psi}dt) & -\sin(\int_{t-\Delta t}^{t}\dot{\psi}dt) \\ \sin(\int_{t-\Delta t}^{t}\dot{\psi}dt) & \cos(\int_{t-\Delta t}^{t}\dot{\psi}dt) \end{bmatrix}}_{E_\delta} \underbrace{\begin{bmatrix} \dot{\psi}^2\cos\psi \\ -\dot{\psi}^2\sin\psi \end{bmatrix}}_{u_d} \tag{4.42}$$

Therefore, the delayed regressor vector has the following relationship with the real disturbance vector

$$u_d = -E_\delta^{-1}E\phi_{dd} \tag{4.43}$$

The nominal value of adaptive gain matrix becomes

$$K^*_{adr} = TE_\delta^{-1}E \tag{4.44}$$

which is a matrix with sinusoidal functions with respect to time when $\dot{\psi}$ is increasing, and becomes a constant matrix when $\dot{\psi}$ reach steady state.

Therefore, the sinusoidal tracking behavior in adaptive gain when there is delay in speed measurement can be explained. However, when the nominal value matrix K^*_{adr} is time-varying, the convergence of adaptive gains will take more time, resulting in a large amplitude in response.

Chapter 5

Conclusions and future work

An adaptive control system capable of rejecting unbalance disturbances for an accelerating rotor supported by active magnetic bearings is presented in this thesis.

In Chapter 2, a state variable description for a transient AMB system under unbalance disturbances is obtained.

In Chapter 3, a desired form of stabilized system is selected. Stability of the system is proved by Lyapunov theory. Local PD controller and centralized PD controller are compared with respect to their performances in realizing the desired closed loop system. The centralized PD controller leads to a better system performances. A method to attenuate gyroscopic effects by a speed-dependent feedback gain matrix is provided.

In Chapter 4, an adaptive controller for the rejection of sinusoidal disturbances with time-varying frequency and time-varying magnitude is designed using Lyapunov theory. Then the adaptive controller is applied to a stabilized AMB system. The P matrix constructed for the Lyapunov equation in Chapter 3 is used for constructing the adaptive control law. Simulation results show its effectiveness in reject unbalance disturbances during acceleration.

In the future, the adaptive controller need to be improved, so that the phase-delay elements can not destabilize the closed loop system. In [2], a method using *augmented error* can maintain the stability of adaptive system when the plant is non-SPR. However, this method is more applicable in SISO system for reference tracking. How to apply this method in MIMO system for disturbance rejection will be an interesting topic to explore.

Bibliography

[1] Markus Ahrens, Ladislav Kučera, and Rene Larsonneur. Performance of a magnetically suspended flywheel energy storage device. *Control Systems Technology, IEEE Transactions on*, 4(5):494–502, 1996.

[2] Karl J Åström and Björn Wittenmark. *Adaptive control*. Courier Corporation, 2013.

[3] Kelly Barber. Health monitoring for flywheel rotors supported by active magnetic bearings. Master's thesis, Auburn University, 2006.

[4] Hannes Bleuler, Matthew Cole, Patrick Keogh, R Larsonneur, E Maslen, Y Okada, G Schweitzer, A Traxler, Gerhard Schweitzer, Eric H Maslen, et al. *Magnetic bearings: theory, design, and application to rotating machinery*. Springer Science & Business Media, 2009.

[5] Jeffrey J DaCunha. Stability for time varying linear dynamic systems on time scales. *Journal of Computational and Applied Mathematics*, 176(2):381–410, 2005.

[6] Robert J Fuentes and Mark J Balas. Direct adaptive rejection of persistent disturbances. *Journal of Mathematical Analysis and Applications*, 251(1):28–39, 2000.

[7] Jerry Ginsberg. *Engineering dynamics*, volume 10. Cambridge University Press, 2008.

[8] James W Jantz. Development of a multi-mode adaptive controller and investigation of gain variations with speed and balance changes. Master's thesis, Auburn University, 2014.

[9] Robert P Jantz. Controlling the speed of a magnetically-suspended rotor with compressed air. Master's thesis, Auburn University, 2011.

[10] Alex Logan Matras. Implementation of adaptive disturbance rejection control in an active magnetic bearing system. Master's thesis, Auburn University, 2003.

[11] Hung Nguyen-Schäfer. *Rotordynamics of automotive turbochargers*. Springer, 2015.

[12] Erik Swanson, Chris D Powell, and Sorin Weissman. A practical review of rotating machinery critical speeds and modes. *Sound and vibration*, 39(5):16–17, 2005.

[13] John M Vance. *Rotordynamics of turbomachinery*. John Wiley & Sons, 1988.

[14] Shiyu Zhou and Jianjun Shi. Imbalance estimation for speed-varying rigid rotors using time-varying observer. *Journal of dynamic systems, measurement, and control*, 123(4):637–644, 2001.

[15] Robert N. Dean, George T. Flowers, Scottedward A. Hodel, Ran Zhou, Simon Castro, Alfonso Moreira, and James Brunsch, "On the Degradation of MEMS Gyroscope Performance in the Presence of High Power Acoustic Noise," presented at the *2007 IEEE International Symposium on Industrial Electronics (ISIE2007)*, Vigo (Spain), June 4-7, 2007.

[16] Alex L. Matras, G.T. Flowers, R. Fuentes, M. Balas, and J. Fausz, "Suppression of Persistent Rotor Vibrations Using Adaptive Techniques," *ASME Journal of Vibration and Acoustics*, December 2006, Vol. 128, No. 6, pp. 682-689.

[17] György Szász and George T. Flowers, "Time Periodic Control of a Bladed Disk Assembly Using Shaft Based Actuation," *ASME Journal of Vibration and Acoustics*, Vol. 123, July 2001, pp. 395-398.

[18] Yasser Gowayed, Faissal Abdel-Hady, George T. Flowers, and Jeffrey J. Trudell, "Optimal design of multi-direction composite flywheel rotors," *Polymer Composites*, Vol. 23, Issue 3, June 2002, pp. 433-441.

[19] Roland Horvath, George T. Flowers, and Jerry Fausz, "Passive Balancing of Rotor Systems Using Pendulum Balancers," *ASME Journal of Vibration, Acoustics, Stress, and Reliability in Design*, 2008, Vol. 130, No. 4, pp. 011011.

[20] V. C. Chancey, G. T. Flowers, and C. L. Howard, "A harmonic wavelet approach for extracting transient patterns from measured rotor vibration data," *46th ASME Gas Turbine and Aeroengine Congress, Exposition, and User's Symposium (ASME Turbo Expo 2001: Power of Land, Sea, and Air)*, June 2001, V004T03A008- V004T03A008.

[21] J. L. Lawen and G. T. Flowers, "Synchronous dynamics of a coupled shaft/bearing/housing system with auxiliary support from a clearance bearing: Analysis and experiment," June 1995, *ASME 1995 Gas Turbine and Aeroengine Congress and Exposition*, V005T14A016-V005T14A016.

[22] G. T. Flowers and S. G. Ryan, "Development of a set of equations for incorporating disk flexibility effects in rotordynamical analyses," June 1991, *ASME 1991 Gas Turbine and Aeroengine Congress and Exposition*, V005T14A008- V005T14A008.

[23] R. Dean, G. Flowers. S. Hodel, K. MacAllister, R. Horvath, A. Matras, G. Robertson, and R. Glover, "Vibration isolation of MEMS sensors for aerospace applications," June 1991, SPIE Proceedings Series, 2002, *Proceedings of the International Conference on Advanced Packaging and Systems*, pp. 166-170.

[24] K. Hornig and G. Flowers, "Parameter characterization of the Bouc/Wen mechanical hysteresis model for sandwich composite materials using real coded genetic algorithms," *International Journal of Acoustics and Vibration*, Vol. 10, No. 2, pp. 73-81.

Appendices

Appendix A

Matrices and vectors

1.

$$M = \begin{bmatrix} I_T & 0 & 0 & 0 \\ 0 & m & 0 & 0 \\ 0 & 0 & I_T & 0 \\ 0 & 0 & 0 & m \end{bmatrix}$$

2.

$$G(\dot{\psi}) = \begin{bmatrix} 0 & 0 & -I_P\dot{\psi} & 0 \\ 0 & 0 & 0 & 0 \\ I_P\dot{\psi} & 0 & 0 & 0 \\ 0 & 0 & 0 & 0 \end{bmatrix}$$

3.

$$B = \begin{bmatrix} L_B & -L_B & 0 & 0 \\ 1 & 1 & 0 & 0 \\ 0 & 0 & -L_B & L_B \\ 0 & 0 & 1 & 1 \end{bmatrix}$$

4.

$$B_d = \begin{bmatrix} m_u u_x u_z & m_u u_y u_z \\ m_u u_x & m_u u_y \\ -m_u u_y u_z & m_u u_x u_z \\ m_u u_y & -m_u u_x \end{bmatrix}$$

5.

$$C = \begin{bmatrix} L_S & 1 & 0 & 0 \\ -L_S & 1 & 0 & 0 \\ 0 & 0 & -L_S & 1 \\ 0 & 0 & L_S & 1 \end{bmatrix}$$

6.

$$K_s = \begin{bmatrix} k_s & 0 & 0 & 0 \\ 0 & k_s & 0 & 0 \\ 0 & 0 & k_s & 0 \\ 0 & 0 & 0 & k_s \end{bmatrix}$$

7.

$$K_i = \begin{bmatrix} k_i & 0 & 0 & 0 \\ 0 & k_i & 0 & 0 \\ 0 & 0 & k_i & 0 \\ 0 & 0 & 0 & k_i \end{bmatrix}$$

8.

$$K_{adr} = \begin{bmatrix} k_{1,1} & k_{1,2} \\ k_{2,1} & k_{2,2} \\ k_{3,1} & k_{3,2} \\ k_{4,1} & k_{4,2} \end{bmatrix}$$

9.

$$A_{ss}(\dot{\psi}) = \begin{bmatrix} 0 & 0 & 0 & 0 & 1 & 0 & 0 & 0 \\ 0 & 0 & 0 & 0 & 0 & 1 & 0 & 0 \\ 0 & 0 & 0 & 0 & 0 & 0 & 1 & 0 \\ 0 & 0 & 0 & 0 & 0 & 0 & 0 & 1 \\ -\frac{2k_s L_B^2}{I_T} & 0 & 0 & 0 & 0 & 0 & \frac{I_P}{I_T}\dot{\psi} & 0 \\ 0 & -\frac{2k_s}{m} & 0 & 0 & 0 & 0 & 0 & 0 \\ 0 & 0 & -\frac{2k_s L_B^2}{I_T} & 0 & -\frac{I_P}{I_T}\dot{\psi} & 0 & 0 & 0 \\ 0 & 0 & 0 & -\frac{2k_s}{m} & 0 & 0 & 0 & 0 \end{bmatrix}$$

10.

$$A_{cl,ss}(\dot{\psi}) = \begin{bmatrix} 0 & 0 & 0 & 0 & 1 & 0 & 0 & 0 \\ 0 & 0 & 0 & 0 & 0 & 1 & 0 & 0 \\ 0 & 0 & 0 & 0 & 0 & 0 & 1 & 0 \\ 0 & 0 & 0 & 0 & 0 & 0 & 0 & 1 \\ -\frac{2k_s L_B^2 + k_{p1}}{I_T} & 0 & 0 & 0 & -\frac{k_{d1}}{I_T} & 0 & \frac{I_P}{I_T}\dot{\psi} & 0 \\ 0 & -\frac{2k_s + k_{p2}}{m} & 0 & 0 & 0 & -\frac{k_{d2}}{m} & 0 & 0 \\ 0 & 0 & -\frac{2k_s L_B^2 + k_{p1}}{I_T} & 0 & -\frac{I_P}{I_T}\dot{\psi} & 0 & -\frac{k_{d1}}{I_T} & 0 \\ 0 & 0 & 0 & -\frac{2k_s + k_{p2}}{m} & 0 & 0 & 0 & -\frac{k_{d2}}{m} \end{bmatrix}$$

11.

$$B_{ss} = \begin{bmatrix} 0 & 0 & 0 & 0 \\ 0 & 0 & 0 & 0 \\ 0 & 0 & 0 & 0 \\ 0 & 0 & 0 & 0 \\ L_B & -L_B & 0 & 0 \\ 1 & 1 & 0 & 0 \\ 0 & 0 & -L_B & L_B \\ 0 & 0 & 1 & 1 \end{bmatrix}$$

12.

$$\bar{B}_{ss} = \begin{bmatrix} 0 & 0 & 0 & 0 \\ 0 & 0 & 0 & 0 \\ 0 & 0 & 0 & 0 \\ 0 & 0 & 0 & 0 \\ 1 & 0 & 0 & 0 \\ 0 & 1 & 0 & 0 \\ 0 & 0 & 1 & 0 \\ 0 & 0 & 0 & 1 \end{bmatrix}$$

13.

$$B_{d,ss} = \begin{bmatrix} 0 & 0 \\ 0 & 0 \\ 0 & 0 \\ 0 & 0 \\ \frac{m_u u_x u_z}{I_T} & \frac{m_u u_y u_z}{I_T} \\ \frac{m_u u_x}{m} & \frac{m_u u_y}{m} \\ -\frac{m_u u_y u_z}{I_T} & \frac{m_u u_x u_z}{I_T} \\ \frac{m_u u_y}{m} & -\frac{m_u u_x}{m} \end{bmatrix}$$

14.

$$C_{ss} = \begin{bmatrix} L_S & 1 & 0 & 0 & 0 & 0 & 0 & 0 \\ -L_S & 1 & 0 & 0 & 0 & 0 & 0 & 0 \\ 0 & 0 & -L_S & 1 & 0 & 0 & 0 & 0 \\ 0 & 0 & L_S & 1 & 0 & 0 & 0 & 0 \end{bmatrix}$$

15.

$$q = \begin{bmatrix} \alpha & X & \beta & Y \end{bmatrix}^\top$$

16.

$$q_b = \begin{bmatrix} X_{1b} & X_{2b} & Y_{1b} & Y_{2b} \end{bmatrix}^\top$$

17.

$$q_s = \begin{bmatrix} X_{1s} & X_{2s} & Y_{1s} & Y_{2s} \end{bmatrix}^\top$$

18.

$$x = \begin{bmatrix} q & \dot{q} \end{bmatrix}^\top$$

19.

$$y = q_s$$

20.

$$i_c = \begin{bmatrix} i_{c1x} & i_{c2x} & i_{c1y} & i_{c2y} \end{bmatrix}^\top$$

21.

$$u_d = \begin{bmatrix} \dot{\psi}^2 \cos\psi + \ddot{\psi} \sin \\ -\dot{\psi}^2 \sin\psi + \ddot{\psi} \cos \end{bmatrix}$$

22.

$$\phi_d = \begin{bmatrix} \Omega^2 \cos(\int_0^t \Omega d\tau) \\ -\Omega^2 \sin(\int_0^t \Omega d\tau) \end{bmatrix}$$

Appendix B

The model data for simulation

Notation	**Description**	**Value**
m	The mass of rotor	6.084 kg
I_T	The transverse moment of inertia of rotor	0.0494 kg·m^2
I_P	The polar moment of inertia of rotor	0.0245 kg·m^2
μ_0	The permeability of free space	1.257e-6 N/A^2
N	The number of coil turns	90
g_0	The distance of air gap	0.00025 m
A_g	The area of gap pole area	0.00118 m^2
i_{bp}	The bias current for the electromagnet on the top	2 A
i_{bn}	The bias current for the electromagnet on the bottom	1.887 A
k_{s1}	The force/displacement factor of magnetic bearing No.1	-2.9069e+6 N/m
k_{s2}	The force/displacement factor of magnetic bearing No.2	-2.9069e+6 N/m
k_{i1}	The force/current factor of magnetic bearing No.1	373.6036 N/A
k_{i2}	The force/current factor of magnetic bearing No.2	373.6036 N/A
u_x	Imbalance mass location parameter 1	0.0354 m
u_y	Imbalance mass location parameter 2	0.0354 m
u_z	Imbalance mass location parameter 3	0.0100 m
L_B	The distance from the center of bearing plane to the center of mass of rotor	0.15 m
L_S	The distance from the center of sensor plane to the center of mass of rotor	0.08 m

Table B.1: The model data for simulation

Appendix C

SIMULINK blocks

A part of the SIMULINK blocks used in computer simulation is shown in this chapter.

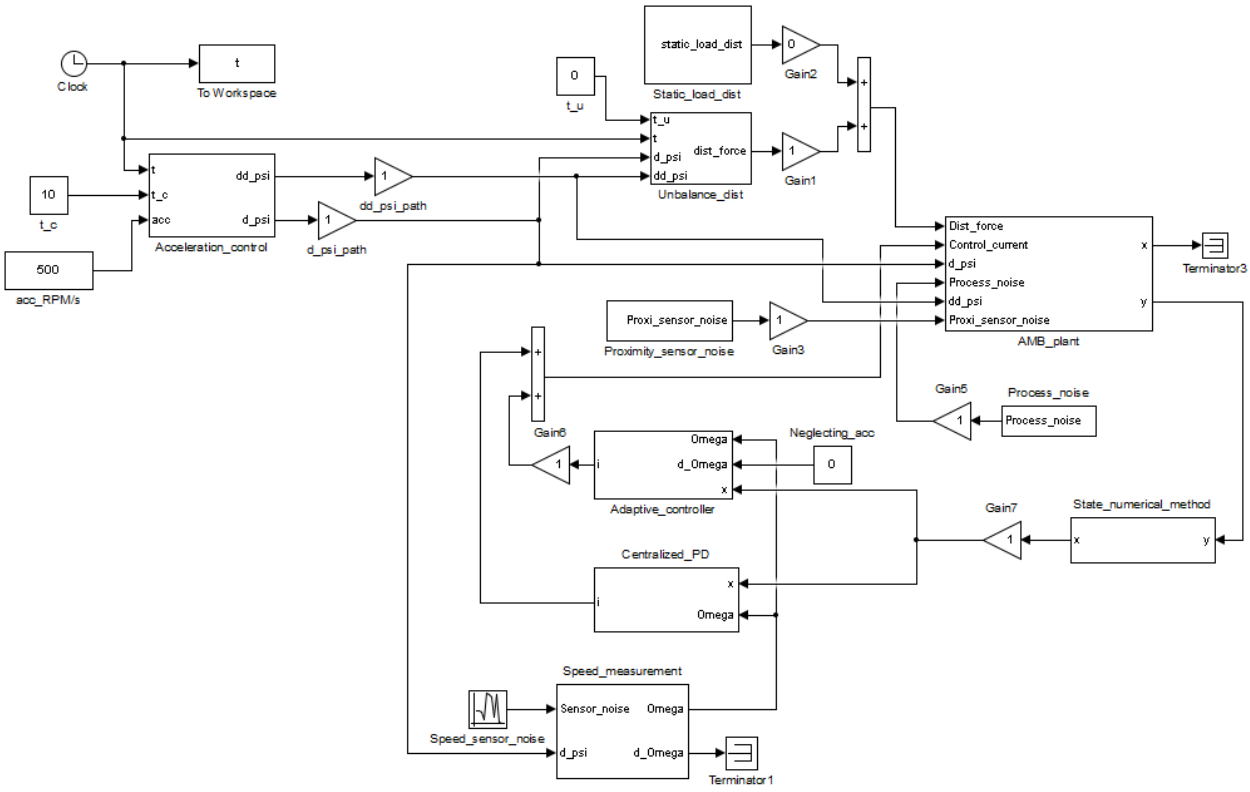

Figure C.1: Overall blocks

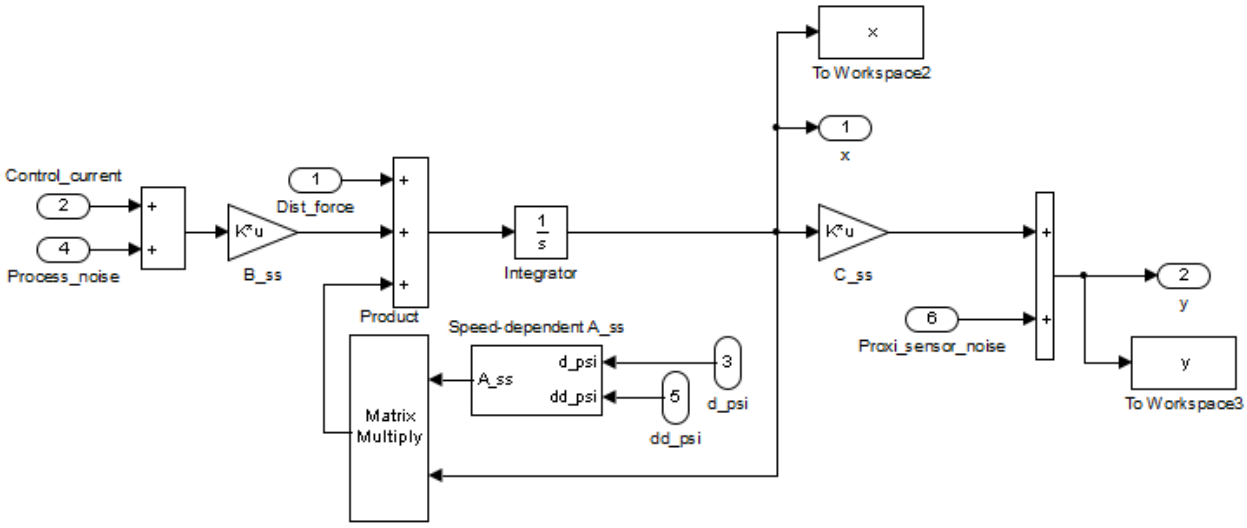

Figure C.2: AMB_plant

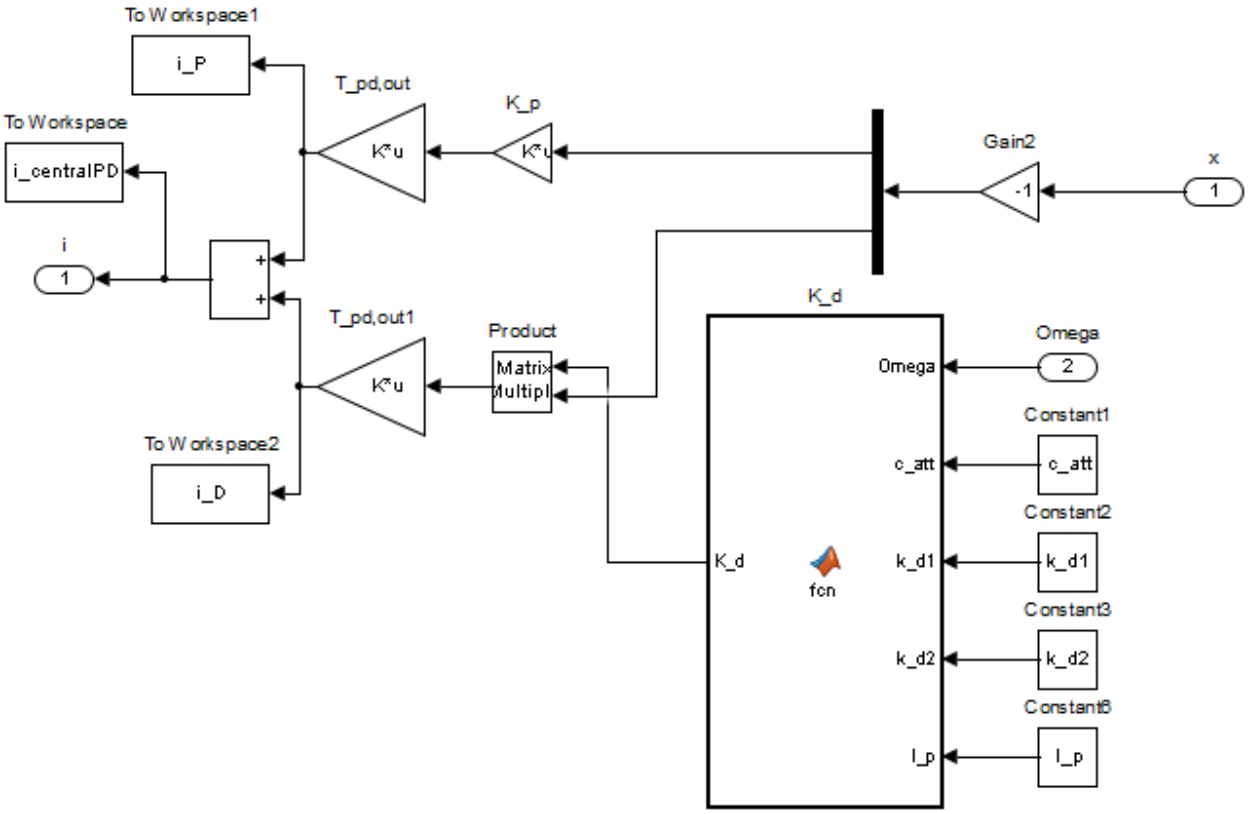

Figure C.3: Centralized_PD

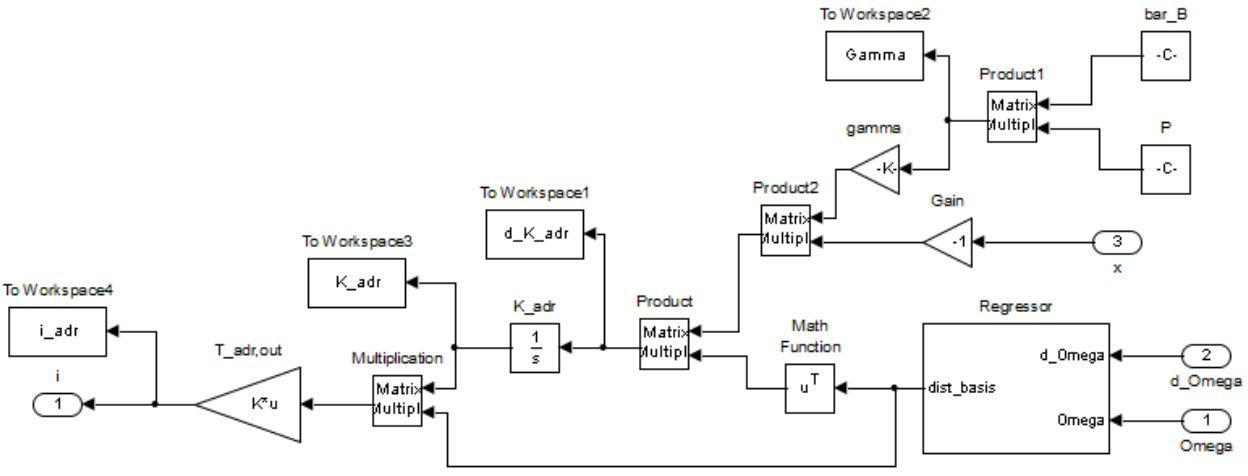

Figure C.4: Adaptive_controller

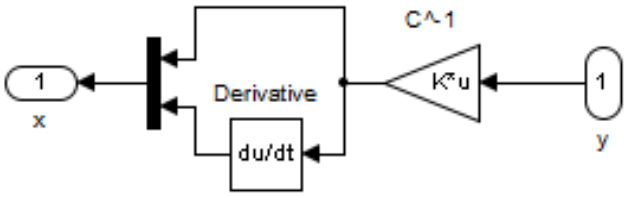

Figure C.5: State_numerical_method

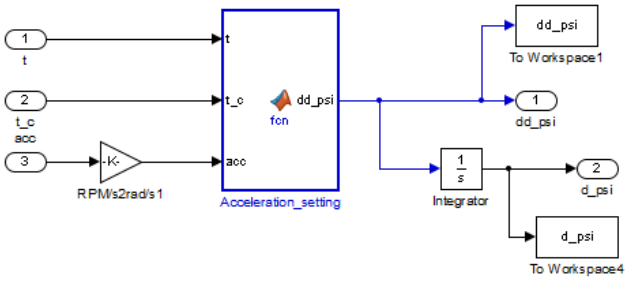

Figure C.6: Acceleration_control

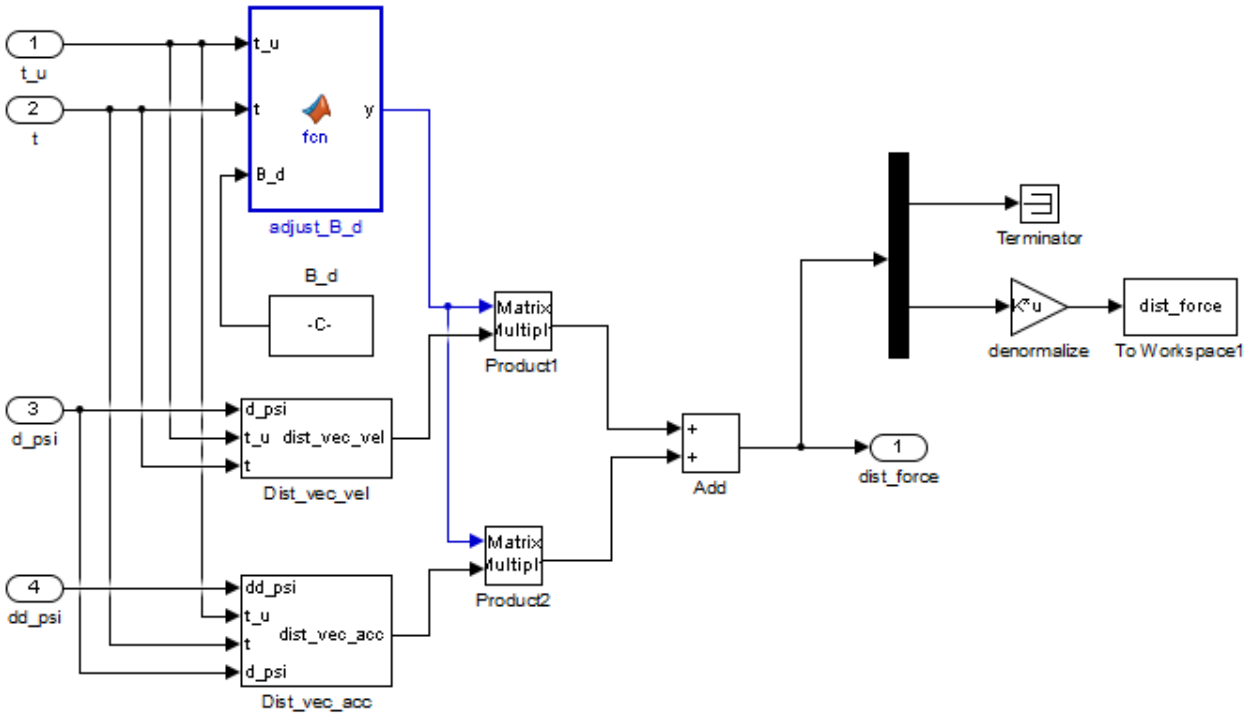

Figure C.7: Unbalance_dist